POLITECNICO DI TORINO

Corso di Laurea in Ingegneria Elettronica

Tesi di Laurea Magistrale

Impact of Transmitter Distortion on Coherent Optical Systems

Relatore
prof. Renato Orta

Correlatore:
prof. Richard Schatz

Laureando
Gabriele Di Rosa
matricola: s239647

Supervisori aziendali
Finisar AB
dott. Jan-Olof Wesström e dott. Robert Lewén

Anno accademico 2018 – 2019

Indice

Elenco delle figure

Abstract

Coherent optical communication systems have the possibility of increasing the channel capacity without the need of raising the bandwidth of the system, which is nowadays becoming a more and more challenging operation. If optical gain through the use of an integrated device is desired the only viable option is the use of a Semiconductor Optical Amplifier (SOA). This device is anyway characterised by a strong non linear response, introducing a distortion on the transmitted signal. As a results the performance of the system rapidly deteriorates for what concerns the Bit Error Rate (BER).

This work will then start with the characterisation of the distortion introduced by a SOA, considering its dependences on the amplifier parameters, the signal characteristics and the device working point.

The model developed for this purpose will be then verified through the use of a commercial software. Attention will be put in observing the impact of the different approximations performed in order to keep the model accurate while avoiding an excessive computational intensity. This last point, in particular, will be the main focus of the model building process since it results essential for its usage as the starting point for the development of DSP based compensation routines.

The next step after this characterisation will be in fact to exploit the obtained knowledge to develop viable methods to correct the SOA induced distortion. The final goal of this compensation is the achievement of a considerable reduction of the obtained BER for high order modulations, which, as it will be shown, often becomes too high for real applications.

For this purpose several methods will be studied, both based on DSP, as anticipated, and on analogue solutions. Each of these will be characterised considering not only the compensation effectiveness but also other factors such as the energetic efficiency and the additive system complexity introduced.

Capitolo 1

Introduction

In this chapter an overview of the subject of this thesis is provided to the reader. In section 1.1 a broad spectrum description of the full optical chain from transmitter to receiver is given. Section 1.2 focuses more specifically on the device of interest for this work, the SOA. Here a theoretical background about both the amplifier's ideal behaviour and its impact on signal distortion are presented.

1.1 Coherent optical systems

Since their introduction in communication systems optical links provided an impressive increase in transmission speed, reaching data rates up to 100 Gbit/s [7]. For a long time the preferred modulation format for such optical systems was On Off Keying (OOK). Mainly two reasons promoted this choice: the inherent low complexity of transmitters and receivers able to work with purely intensity based modulation and the conspicuous error margin which positively affects the obtained BER.

Nowadays the interest in improving the channel capacity, together with the difficulty in increasing the bandwidth, has instead brought attention to higher order modulation formats. The most commonly used being M levels Pulse Amplitude Modulation (M-PAM), Phase Shift Keying (M-PSK) and Quadrature Amplitude Modulation (M-QAM). While with OOK only one bit at a time is sent, using these modulation formats several bits per symbol are transmitted, resulting in a much higher spectral efficiency. The use of these modulation schemes has anyway drawbacks from different points of view: complex Photonic Integrated Circuits (PIC), able to manage both amplitude and phase of the signal, are required, DSP at the receiver is needed and the error margins are reduced.

The full system simulated in this work can be schematically described as represented in figure 1.1.

1.1.1 M-QAM format

M-QAM is of particular interest for this work because of its possibility of reaching high spectral efficiency with $\ln_2(M)$ bits transmitted for each symbol. This modulation format

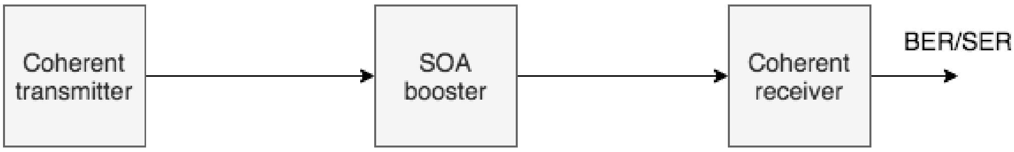

Figura 1.1. Block diagram including the main components of a coherent communication system.

is achieved through the combination of two amplitude modulated carriers, I and Q, which are in phase quadrature. This is at least valid for rectangular QAM, which is the format used throughout this work. The I and Q components are combined and sent through the communication link to then be separated again at the receiver stage. Compared to M-PSK and M-PAM, while achieving the same bits per symbol and constellation energy, higher levels separation is obtained with M-QAM. This is the main reason why it is the common choice for high order modulation formats. In figure 1.2 the constellations relative to these three different schemes, with M=16, are shown for comparison.

Increasing M reflects in an higher spectral efficiency but in reduced decision margins, worsening the BER, or equivalently the Symbol Error Rate (SER). In high speed optical communications at the moment in which this work is written 16-QAM systems are commercially available and 64-QAM is an active research topic. In this project then these are the two modulation formats of interest. OOK is also used during model building and benchmarking because of its simplicity, which helps visualisation and understanding of the phenomena of interest.

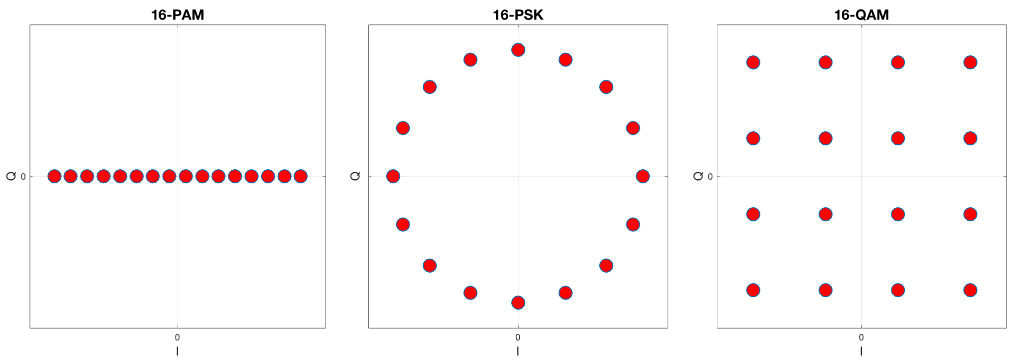

Figura 1.2. 16-PAM, 16-PSK and 16-QAM constellations in the I-Q plane.

1.1.2 Coherent optical transmitter

Different layouts have been developed to obtain multi-level modulations. M-PSK and M-QAM, in particular, can be obtained with the same device just through a proper choice of the electric driving signals.

A common approach is to split the input optical power into two components I and Q with 90° phase difference. At this point these are properly amplitude and phase modulated before getting combined to form the desired transmitted signal. Two block diagrams representing circuits of this kind, taken from [8], are here reported in figure 1.3.

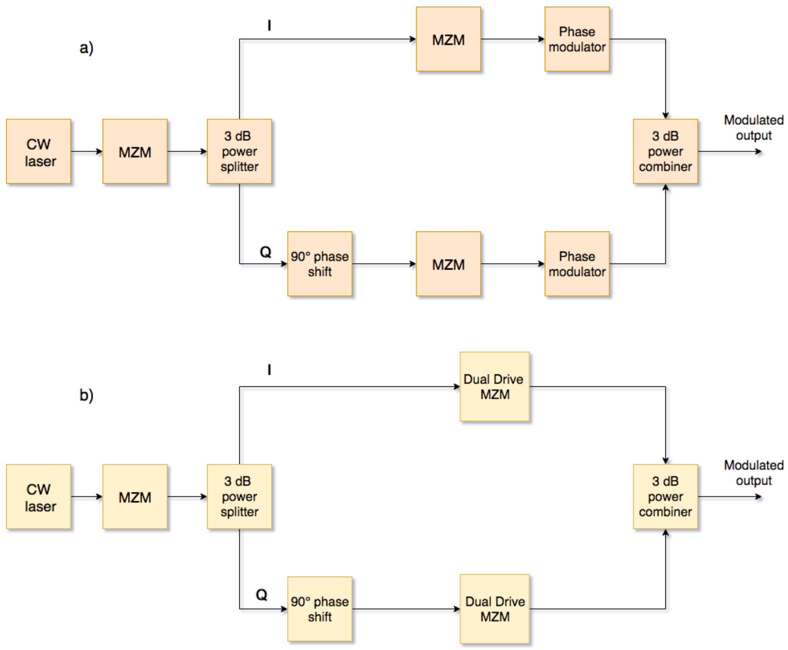

Figura 1.3. Two examples of coherent transmitters.

In layout a) the in-phase and quadrature components are sequentially amplitude and phase modulated. On the contrary in b) the use of a dual-drive Mach-Zender Modulator (MZM) allows to perform these two steps at the same time, thus reducing the number of stages but increasing the complexity of the driving circuitry. The architecture choice influences the impact of the different error sources that make the output signal not ideal. In this work anyway non idealities introduced by the transmitter are not taken into account since the focus is on the impact of the SOA on the system.

1.1.3 Coherent optical receiver

To retrieve information about both amplitude and phase of the received signal the idea is once again to separate the I and Q components. These can be obtained through the use of a laser as a reference Local Oscillator (LO) whose output is properly coupled with the received signal. A block diagram of a coherent receiver is shown in figure 1.4.

As already stated regarding the transmitter also for this device many architectures are possible [9], leading to a different influence of errors such as I-Q imbalance. In this work, anyway, an ideal behaviour is assumed.

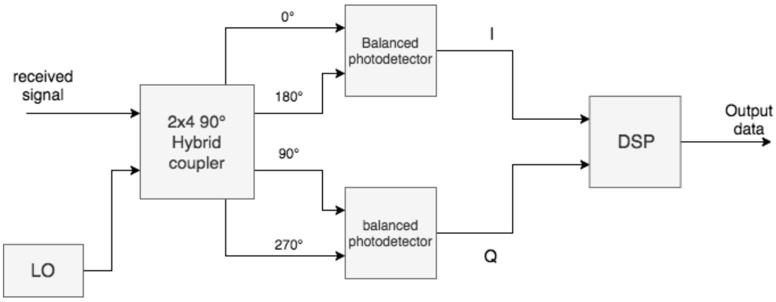

Figura 1.4. Block diagram of a coherent receiver.

1.2 Theoretical background on SOAs

1.2.1 Why SOAs?

In many situations it is needed to amplify optical signals. The two most common solutions are represented by using an Erbium Doped Fibre Amplifier (EDFA) and a SOA. EDFAs have many advantages for what concerns chirp, pulse distortion and noise figure with respect to SOAs but they are not suitable for integration. Then if optical gain is needed in an integrated device using a SOA becomes the only option available.

One typical PIC in which amplification is needed is the optical transmitter. In this system a booster SOA is a suitable and efficient way to overcome the modulator induced loss [10].

1.2.2 Ideal working principle

A SOA can be thought simply as a Fabry-Perot cavity. An active semiconductor layer is pumped through an injected current I_{SOA} in order to achieve a certain optical gain. It is at this point possible to distinguish between two categories of SOAs:

1. Fabry-Perot Semiconductor Optical Amplifier (FP-SOA), whose facets show considerable reflectivity. Because of multiple reflections the gain spectrum is characterised by strong ripples. Moreover the device is sensitive to current, temperature fluctuations and signal polarization.

2. Travelling Wave Semiconductor Optical Amplifier (TW-SOA), whose facets have very small reflection coefficients (up to 10^{-5}). In this case the input signal is ideally subject to a single pass gain only. This results in a considerable improvement in all the problems highlighted regarding FP-SOAs [1].

Because of its better performance, in particular regarding the device bandwidth, TW-SOAs are the most common choice. From now on only this device will be considered and it will be just referred to as SOA for brevity.

The device structure of a double heterostructure SOA is shown in figure 1.5, together with the band diagram through a cross section along the y-axis. Where the band gap is smaller the refractive index is higher, this results in the structure confining both carriers and optical field in the active region, where the signal propagates and gets amplified. The positive z-axis is arbitrarily taken as the field propagation direction in the following of this work.

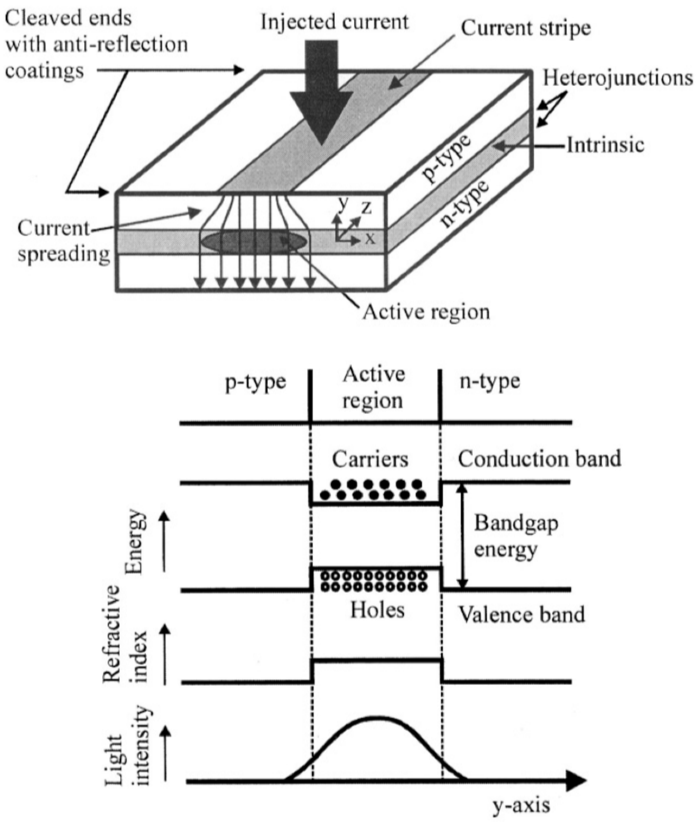

Figura 1.5. SOA structure and band diagram along the y-axis (Figure from [1]).

The single pass power gain has an exponential dependence on the device length L, the material gain $g(N)$, where N is the carrier density in the active region, and the confinement factor Γ:

$$G(t) = \frac{P(z = L, t)}{P(z = 0, t)} = \mathrm{e}^{\Gamma L g(N)}. \tag{1.1}$$

For ideal operation it is desired to have in steady-state conditions a constant gain

$$G(t) = G_{ss} = \mathrm{e}^{\Gamma L g(N_{ss})}. \tag{1.2}$$

To evaluate N the carrier rate equation in the SOA active layer can be written as in [11]:

$$\frac{dN}{dt} = \frac{\eta_i I_{SOA}}{qV} - \frac{N}{\tau_c} - g(N)\frac{P(t)\Gamma}{Vh\nu}, \tag{1.3}$$

where η_i is the current injection efficiency, q is the elementary charge, V is the active region volume, P is the optical power, τ_c is the spontaneous carrier lifetime, ν is the optical field frequency and h is Planck's constant.

If the third term of the right hand side in (1.3) is negligible it is easy to find the steady state carrier density as:

$$N_{ss} = \frac{\eta_i I_{SOA} \tau_c}{qV}, \tag{1.4}$$

this value can finally be inserted in (1.2) to obtain the time independent single pass power gain of the device. Unfortunately it is evident that this ideal condition fails if this power dependent term is not negligible. In this case the carrier density in the active region fluctuates, following a time dependence imposed by the variable optical field travelling in the SOA. This phenomenon is at the basis of the induced distortion which is of interest for this work, which will be now described in detail.

1.2.3 SOA induced distortion

Carrier density fluctuations have different impacts on the signal propagating in the device. For the moment the material gain is evaluated through a linear model, which is suitable for bulk SOAs, as:

$$g = a(N - N_{tr}), \tag{1.5}$$

where $a = dg/dN$ is the differential gain and N_{tr} is the transparency level of the carrier density. This last is the value of N for which the device has a material gain exactly equal to zero and thus a single pass gain of exactly one, characterising transparency.

If the carrier density does not reach a fixed steady-state value but, on the contrary, follows a time dependency based on the propagating signal, it can be observed how the gain is also subject to fluctuations. This phenomenon is known as gain saturation and introduces a distortion since the signal is not amplified of the same factor in every time instant.

This change in the carrier density affects not only the gain but introduces also fluctuations in the material refractive index n, through the following dependency:

$$n = \sqrt{n_b^2 - \frac{\bar{n}\lambda_0}{2\pi}(\alpha + i)g(N)}, \tag{1.6}$$

where n_b is the background refractive index, function of the cross-section, $\bar{n}$ is the effective mode index, λ_0 is the optical field wavelength and α is the linewidth enhancement factor.

Gain saturation then is also related to a non constant phase shift during the signal propagation, which translates in the introduction of a frequency chirp. This phenomenon takes the name of Self Phase Modulation (SPM).

It is easy to observe the effects of gain saturation looking at a single Gaussian pulse propagated through a SOA as in figure 1.6.

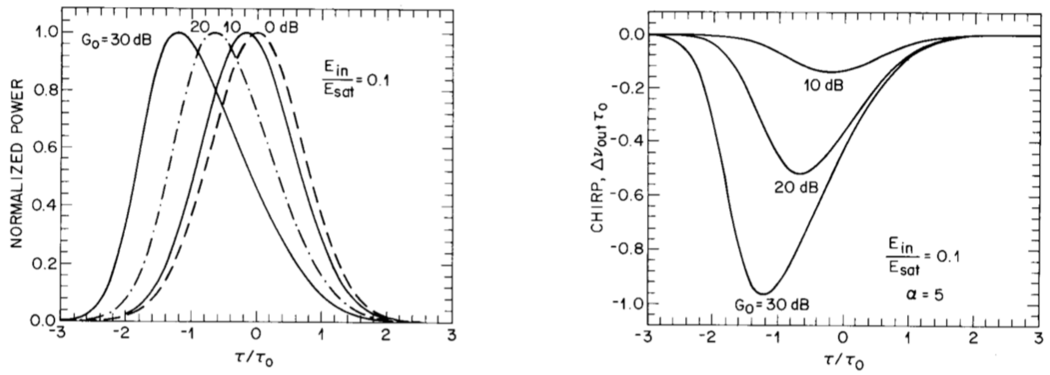

Figura 1.6. Effect of gain saturation on a Gaussian pulse travelling through the SOA (Figure taken from [2]).

Where the axis of abscissae is referred to a moving time frame $\tau = t - L/v_{group}$ normalized to the pulse Full Width Half Maximum (FWHM) τ_0 for obtaining a good visualisation of the phenomenon.

The pulse energy in this example is equal to one tenth of what is referred to as the device saturation energy:

$$E_{sat} = \frac{h\nu\sigma}{a}, \tag{1.7}$$

where σ is the mode cross section.

With such a value the time dependent term of (1.3) is not negligible and a visible distortion is obtained. From the plots of the output waveform it is possible to observe the typical distorted pulse shape, characterised by the leading edge being sharper than the trailing one. Optical amplification of the incoming signal in fact drains rapidly the carriers in the active region. Because of this the trailing edge experiences lower gain due to the reduced availability of carriers able to take part to the stimulated emission process.

This effect is particularly evident if the pulse period is of the order of the spontaneous recombination lifetime τ_c. In this situation carriers start to repopulate the region together with the pulse travelling, increasing the N variability during the propagation. On the contrary if the pulse period is much longer than τ_c carriers have time to repopulate and a symmetric shape with a widened peak is observed. This effect is known as gain recovery and its enhancement is often a desired feature during SOA design. Finally when the pulse period is much smaller than τ_c on average the signal does not feel a strong carrier density variation and the distortion is reduced.

Concerning the frequency chirp a similar analysis can be carried out: a red shift depending on the signal power is imposed and the effect of gain saturation, as evident from figure 1.6, becomes more important together with the gain increasing. Given the same input power, stronger amplification results in fact in a larger power propagating in the SOA. This, in turn, causes the carrier density to fluctuate up to a greater extent.

Capitolo 2

Modelling of SOA distortion

After having introduced the theory needed to understand the distortion induced by SOAs it is desired to create a simple model to predict this phenomenon. In [2] a good theoretical framework regarding this topic is given and it is then used as the main theoretical reference. During the model building process it is important to keep the model not computationally intensive while guaranteeing a good degree of approximation. This requirement is given by the fact that one of the purposes of the model is to be the basis for a DSP routine able to correct the impairment introduced by a SOA. Coding and simulations for this purpose are all performed in MATLAB.

2.1 Model building

2.1.1 Model equations derivation

If the pulse width of the transmitted signal is much longer than the intra-band relaxation time, which reaches at most values around 0.1 ps, the optical field propagation can be described through rate equations. This assumption is not limiting for the purposes of this work since the baud rate for making this approximation failing should be over 100 GBd/s. For such high values DSP would be anyway prevented by the maximum analog to digital conversion speed achievable. It is then possible to describe field propagation in the SOA as:

$$\frac{\partial N}{\partial t} = \frac{I_{SOA}}{qV} - \frac{N}{\tau_c} - \frac{a(N - N_{tr})}{h\nu}|E|^2, \tag{2.1}$$

where E is the propagating optical field. The injection efficiency η_i is here not introduced and thus the current in the SOA is assumed as the total injected one. Moreover carrier diffusion is neglected since usually the amplifier's width (W) and thickness (t) are much shorter than the diffusion length, while on the contrary the amplifier length (L) is on a much larger scale. The material gain model used is the linear one already defined in (1.5).

Assuming single mode propagation and linear polarization the optical field can be written as:

$$E(x,y,z,t) = \frac{1}{2}\left(M(x,y)A(z,t)\mathrm{e}^{i(k_0 z-\omega_0 t)} + \text{c.c.}\right)\hat{x}, \tag{2.2}$$

where $\hat{x}$ is the polarization unit vector, M is the mode distribution, $k_0 = \bar{n}\omega_0/c$, and $A = \sqrt{P}\mathrm{e}^{i\phi}$ is the signal's envelope. In this last definition P represents the signal power and ϕ its phase.

Using the slowly varying envelope approximation and neglecting internal losses, since usually the gain of the amplifier is much higher, it is then possible to describe the evolution of $A(z,t)$ as:

$$\frac{\partial A}{\partial z} + \frac{1}{v_g}\frac{\partial A}{\partial t} = \frac{i\omega_0\Gamma}{2\bar{n}c}\chi A, \tag{2.3}$$

where v_g is the group velocity, $\chi = n^2 - n_b^2$ is the susceptibility of the active layer material and Γ is the confinement factor, defined as:

$$\Gamma = \frac{\int_0^d \int_0^W |M(x,y)|^2 dxdy}{\int_{-\infty}^{+\infty}\int_{-\infty}^{+\infty} |M(x,y)|^2 dxdy}. \tag{2.4}$$

If the linear gain model is used it is possible to spatially average (2.1) over the active region since N has a spatial dependence but it appears only as a linear term in the equation. Performing this operation the rate equation can be written as:

$$\frac{\partial N}{\partial t} = \frac{I}{qV} - \frac{N}{\tau_c} - \frac{\Gamma g(N)}{h\omega_0 V}\int_0^L P(z)dz. \tag{2.5}$$

To shorten the notation it is convenient to redefine the gain as $g = \Gamma g$ and to rewrite (2.5) as:

$$\frac{\partial g}{\partial t} = \frac{g_0 - g}{\tau_c} - \frac{g}{E_{sat}L}\int_0^L P(z)dz, \tag{2.6}$$

where it must be recalled that $E_{sat} = h\nu\sigma/a$, $\sigma = Wd/\Gamma$ and g_0 is defined as:

$$g_0 = \Gamma a N_{tr}\left(\frac{I_{SOA}}{I_{tr}} - 1\right). \tag{2.7}$$

I_{tr} in this formula is the transparency value of the current injected in the SOA and it is found as $I_{tr} = qVN_{tr}/\tau_c$. For values lower than this optical gain is not achieved.

At this point combining (2.3), (2.6), (1.6) and the respective definitions for χ and g it is possible to write a set of three simple equations describing the field evolution in the SOA:

$$\frac{\partial P}{\partial z} = gP, \tag{2.8}$$

$$\frac{\partial \phi}{\partial z} = -\frac{1}{2}\alpha g, \tag{2.9}$$

$$\frac{\partial g}{\partial t} = \frac{g_0 - g}{\tau_c} - \frac{gP}{E_{sat}L}. \tag{2.10}$$

In the correct formulation of this analysis t should be substituted with $\tau = t - L/v_g$ to take care of the propagation time inside the SOA. Since the term L/v_g represents anyway just a delay it is here avoided for simplicity and will be added while plotting the results only.

Starting from this set of three equation and through the definition of a convenient parameter representing the integrated gain over the device length:

$$h(t) = \int_0^L g(z,t)dz, \tag{2.11}$$

it is finally possible to write a system of equations describing the input-output relation for the signal power and phase. These three equations are the mathematical framework on which the model is based:

$$\frac{dh}{dt} = \frac{g_0 L - h}{\tau_c} - \frac{P_{in}(t)}{E_{sat}}\left(\mathrm{e}^h - 1\right), \tag{2.12}$$

$$P_{out}(t) = P_{in}(t)\mathrm{e}^{h(t)}, \tag{2.13}$$

$$\phi_{out}(t) = \phi_{in}(t) - \frac{1}{2}\alpha h(t). \tag{2.14}$$

2.1.2 Spontaneous lifetime estimation

After having defined the needed equations there is still an observation to make about one of the parameters of the ODE before proceeding to the numerical implementation. The spontaneous lifetime τ_c is in fact usually evaluated through the polynomial approximation:

$$\tau_c = \frac{1}{A + BN(t) + CN(t)^2}, \tag{2.15}$$

where A,B and C are coefficients respectively taking into account linear, bimolecular and Auger recombination. This parameter is then clearly time varying, being dependent on the spatially averaged carrier density $N(t)$. In order to keep the model efficient it is anyway necessary to assign a single value to this parameter. Updating it at every time step would, as a result, make the model significantly slower and not any more adequate for a DSP implementation.

Before solving for all the time points t_i the ODE, an equivalent steady state spatially averaged carrier density N_{ss} is then evaluated. The idea is to find this value solving (2.5) in steady-state conditions with time averaged input power as $P(z)$. The equation to solve thus becomes:

$$\frac{\partial N}{\partial t} = \frac{I}{qV} - \frac{N}{\tau_c} - \frac{\Gamma a(N - N_{tr})}{h\omega_0 V}\int_0^L P_{av,in}\mathrm{e}^{\Gamma a(N-N_{tr})z}dz = 0. \tag{2.16}$$

To find the solution an iterative method is suggested in [12]. This routine is described by the flow diagram in figure 2.1. Here the term to be equalled to zero in (2.16) is called $f(N)$ for brevity.

The basic idea of the method is to start imposing the transparency value as carrier density and to modify N through a weight which is reduced every time $f(N)$ changes sign.

This weight is used to multiply or divide by a factor (1+Weight) the estimation, depending if in the current iteration the tested N led to positive or negative values of $f(N)$. When an ulterior iteration does not lead to a considerable change in the estimated N the loop is finally stopped.

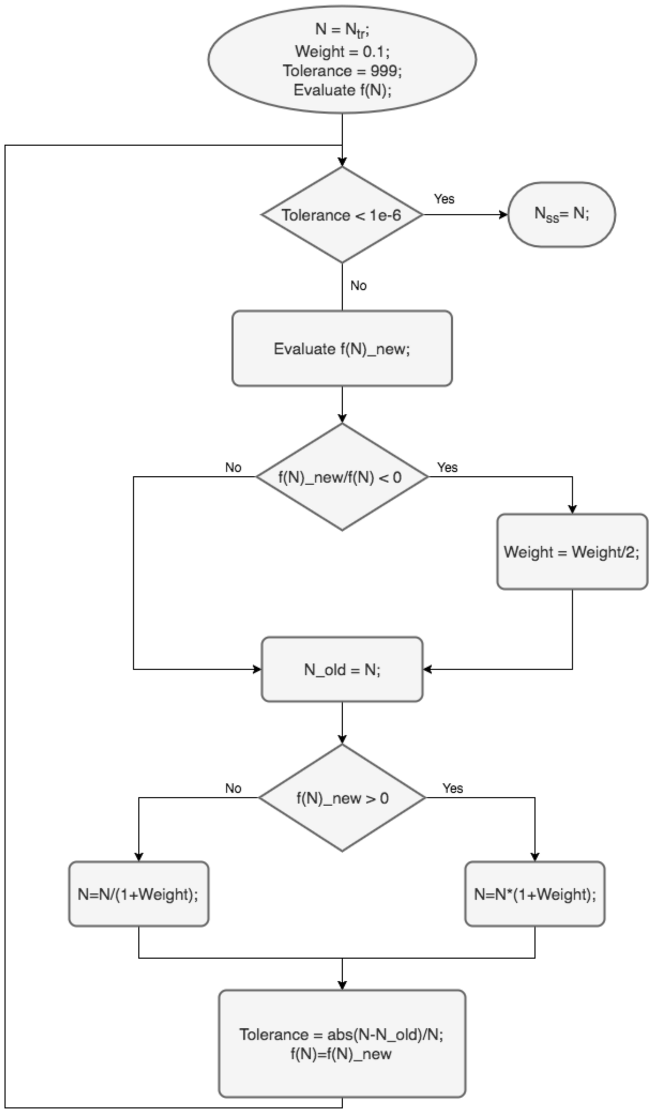

Figura 2.1. Flow diagram if τ_c estimation algorithm.

2.1.3 Model implementation

To find the output waveform, given a certain input field, it is sufficient to solve the differential equation (2.12) in the time range of interest starting from a certain initial condition $h(\tau = 0)$. The output field is then found easily by means of (2.14) and (2.13). To solve

(2.12) anyway numerical methods must be used. For the moment this operation is performed through the built in MATLAB ODE solver routines. For what concerns the initial condition this is set as:

$$h(\tau = 0) = h(t = L/v_g) = \frac{g_0 L}{1 + \frac{\max(P_{in})}{P_{sat}}}, \tag{2.17}$$

where $P_{sat} = E_{sat}/\tau_c$.

The condition with zero optical power in the device would be just $h = g_0 L$ but since the study at the device output starts at time $t = L/v_g$, when the signal has already travelled through the SOA, the material gain is inhomogeneous because of saturation induced by the propagating field. Dividing for the factor $1 + \max(P_{in})/P_{sat}$ helps then improving the convergence of the solution since it brings the starting point to a more realistic value using only known parameters.

2.2 Validation of the model

The simple model developed needs at this point to be validated through comparison with an established simulation tool. The choice for this purpose is to use VPIphotonics Design Suite. This is a commercial software able to simulate optical communication systems in time domain with spatial segmentation through the use of a transmission line model approach. The suite also offers many built-in components, such as M-QAM transmitters and receivers with DSP routines and SER estimation techniques, that are utilised throughout this work. One last feature that makes this software convenient for the project is having the possibility to integrate MATLAB functions in the VPIphotonics environment. This allows to create a single simulation bench in which the data can be at the same time manipulated through the user's code and VPIphotonics proprietary DSP routines.

2.2.1 Device parameters

In order to test the model a fictitious device is created. The parameters characterising it are mostly taken from [12] and will be kept constant if not differently specified throughout this work. Their values are here reported:

- $f_0 = 193.1\,\mathrm{THz}$
- $a = 8.5 \times 10^{-20}\,\mathrm{m}^2$
- $N_{tr} = 1.15 \times 10^{24}\,\mathrm{m}^{-3}$
- $d = 0.4\,\mu\mathrm{m}$
- $W = 0.4\,\mu\mathrm{m}$
- $L = 700\,\mu\mathrm{m}$
- $\Gamma = 0.22$
- $A = 1 \times 10^{9}\,\mathrm{s}^{-1}$
- $B = 1 \times 10^{-16}\,\mathrm{m}^3\,\mathrm{s}^{-1}$
- $C = 1.3 \times 10^{-41}\,\mathrm{m}^6\,\mathrm{s}^{-1}$
- $\alpha = 4$

2.2.2 Comparison of results with alternated OOK input signals

The basic simulation bench created in VPIphotonics is shown in figure 2.2:

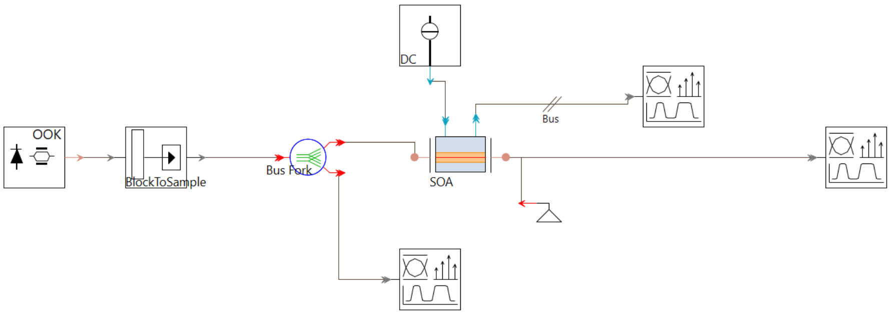

Figura 2.2. Simulation bench in VPIphotonics Design Suite for the simulation of SOA induced distortion on transmitted OOK modulated signals.

This setup is simply based on the SOA to model, an ideal DC current source, an OOK transmitter, a data conversion block needed for the software operation and some signal analysers to observe the simulation results. The parameter of the transmitter are chosen in order to represent a realistic case and give an output signal characterised by:

- $P_1 = 887\,\mu W$ (signal power when a logical 1 is transmitted)
- $P_0 = 113\,\mu W$ (signal power when a logical 0 is transmitted)
- Bit rate = 10 Gbit/s

All the non idealities such as the source laser's linewidth, modulator's insertion loss and so on are neglected. For the moment also no pulse shaping is applied to the transmitted signal.

With this setup different simulations are run modifying the injected current. Tuning this parameter has in fact a major impact on the optical gain obtained and then on the distortion introduced. With this test it is of interest to observe the agreement between the model developed and the commercial software for different distortion levels. To perform a reliable comparison VPI's transmitted signal data are stored in a text file which is used as the input of the MATLAB code. In figures 2.3, 2.4 and 2.5 results for increasing distortion levels are shown.

For a value of injected current just slightly above $I_{tr} \approx 21\,\text{mA}$, as in figure 2.3, an optical gain of only 5 dB is obtained. This leads to a small distortion in the output signal intensity. In this situation the two models show a very good agreement. When the current is increased, as in figure 2.4, the effect of gain saturation starts to be evident: the leading edge is strongly amplified but then the device has no carriers left to sustain the amplification level and the signal intensity gradually decreases. For what concerns the simulation results, anyway, still very good agreement is obtained, with just a small discrepancy around the peak of amplification. In a limit case, as in figure 2.5, characterized by a very strong distortion, the behaviour of the model is still satisfying. Some deviations from VPIphotonics simulation are anyway noticeable.

After this comparison it is then possible to conclude that the simple model coded in MATLAB shows good performance in evaluating the distortion in the output signal's intensity for repetitive patterns.

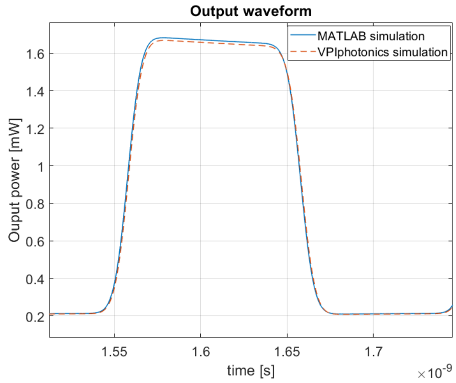

Figura 2.3. Output power comparison for $I_{SOA} = 25\,\mathrm{mA}$ and $G \approx 5.5$ dB.

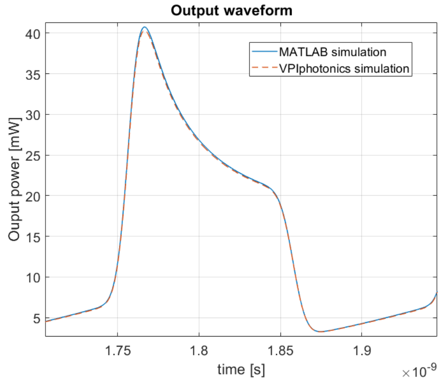

Figura 2.4. Output power comparison for $I_{SOA} = 50\,\mathrm{mA}$ and $G \approx 18$ dB.

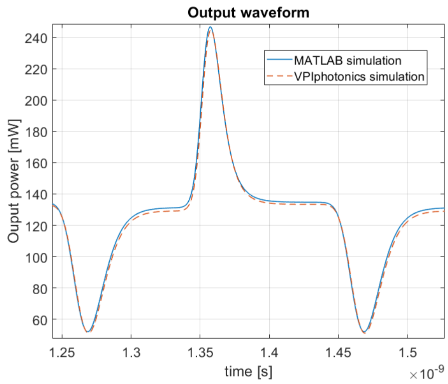

Figura 2.5. Output power comparison for $I_{SOA} = 200\,\mathrm{mA}$ and $G \approx 25$ dB.

2.2.3 Comparison with randomly patterned input signals

Since the final interest is to interface the model with generic QAM signals, a pseudo random 16-QAM input with average power $P_{in,av} = 200\,\mathrm{\mu W}$ is used for this final validation. In this way it is possible to observe if the model correctly follows the pattern dependency of the output signal intensity. The result, obtained as in the previous simulations, is shown in figure 2.6. As it is possible to see the model manages to simulate the pattern effect up to a very good accuracy level.

Looking at figure 2.6 an interesting qualitative insight of the pattern effect can also be obtained. Let us focus for example on the two highest peaks, situated approximatively at $t_{peak,1} = 1.05\,\mathrm{ns}$ and $t_{peak,2} = 1.2\,\mathrm{ns}$. The two input symbols are characterised by the same intensity but the output peaks have different amplitudes. This is due to the fact that the second one is subject to a higher gain saturation induced by the first peak to have drained a very high number of carriers, which still did not completely repopulate the active region.

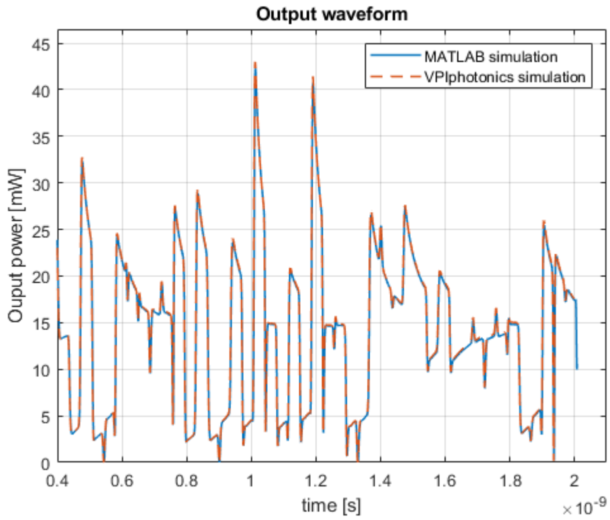

Figura 2.6. Comparison between models for $I_{SOA} = 50\,\text{mA}$, baud rate 28 GBd/s, $G \approx 20$ dB.

2.2.4 Approximation check

The model developed is simple and computationally efficient because it accepts some strong approximations. The main ones being:

1. Reflections at the SOA facets are neglected.
2. The effect of Amplified Spontaneous Emission (ASE) on distortion is not considered.
3. The device is not spatially segmented, resulting in effects like spatial hole burning not being taken into account.
4. The spontaneous lifetime is set to a fixed estimated value and not instantaneously dependent on the carrier density.

These four approximation are now checked through simulations in VPIphotonics, in which all these effects can be taken into account or not. While evaluating the performance of the model with respect to the approximations the typical device operating conditions must be considered: for a booster SOA used in telecommunication system a reasonable request is to achieve a gain of around 10 dB for an input average power of approximatively -10 dBm. This condition is taken as the standard operating point in the following of this text if not differently stated. For what concern frequency and modulation format in this chapter a 10 GHz alternated OOK signal is used.

Effect of facets reflectivity

In a TW-SOA the device's facets are anti-reflection coated in order to achieve very low reflectivity values. It must be anyway stated that it is not possible to achieve exactly zero reflections. In presence of very high power levels in the device, resonances in the Fabry-Perot cavity are observed. This phenomenon leads to supplementary distortions which are not taken into account by the model, thus introducing an estimation error. It is important then to study how the waveform changes with the reflectivity and signal power level in the SOA. In figure 2.7 the effect of reflections is evaluated for $P_{in,av} = -3$ dBm while a more limiting situation, with a much higher input power $P_{in,av} = 15$ dBm, is shown in figure 2.8.

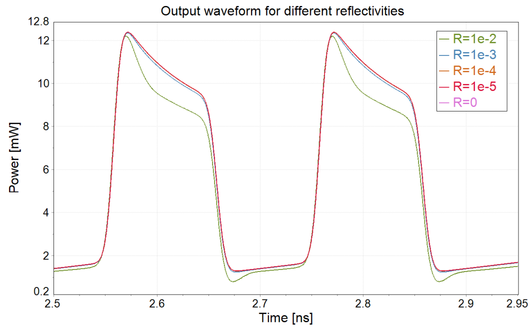

Figura 2.7. Influence of the facets reflectivity on the output waveform for $I_{SOA} = 35\,\text{mA}$ and $G \approx 10$ dB.

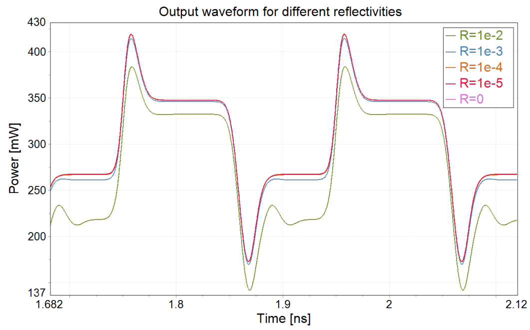

Figura 2.8. Influence of the facets reflectivity on the output waveform for $I_{SOA} = 350\,\text{mA}$ and $G \approx$ 10 dB.

From figure 2.7 it is possible to appreciate how for reflectivity values up to $R = 1 \times 10^{-3}$ no significant difference is observed in the distortion.

In the case in which much higher power is travelling through the SOA, as in figure 2.8, reflectivity plays a bigger role and also for $R = 1 \times 10^{-3}$ a certain discrepancy is noticeable. For lower values anyway the situation looks still close to ideal.

In real commercial devices it is possible to achieve a reflectivity as low as 1×10^{-5}. What the simulations just shown suggest is then that this approximation should not introduce any problems in the model, also for high power levels in the SOA.

Effect of amplified spontaneous emission

ASE can give an important contribution to the SOA distortion since it represent an additive source of optical energy in the active region. This effect can become dominating up to the point that in some modern devices saturation is induced in a controlled way through a very strong ASE [13]. For a simplified analysis of this phenomenon it is reasonable to think for it to be dependent on the injection current only. I_{SOA} is in fact the main source of carrier which become available to spontaneously recombine.

The recombination rate r_{sp} can be approximated as:

$$r_{sp} = n_{sp}\Gamma v_g g(N), \tag{2.18}$$

where n_{sp} is a figure of merit characterizing recombination called inversion parameter. Its value is related to the carrier densities in conduction and valence band and can be approximated as $n_{sp} = N/(N - N_{tr})$.

To check the importance of this effect in the model, different simulations are run with inversion parameter $n_{sp} \in [1;8]$. The setup is the same used until now with the only addition of an optical passband filter after the SOA. The bandwidth of this component is equal to four times the bit rate and it is centred around the optical carrier frequency. In this way it is possible to appreciate only the distortion without visualising the superimposed noise generated by spontaneous emission. In figure 2.9 a current of 35 mA is injected while a much higher value of 350 mA is tested in the simulation shown in figure 2.10.

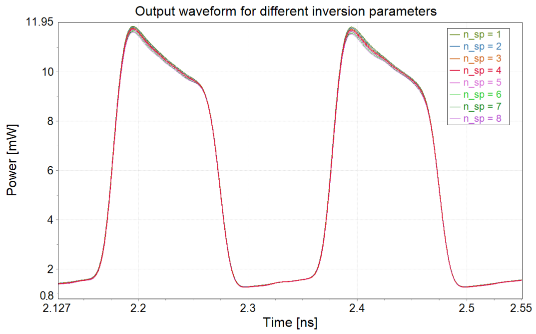

Figura 2.9. Influence of amplified spontaneous emission for $I_{SOA} = 35\,\mathrm{mA}$.

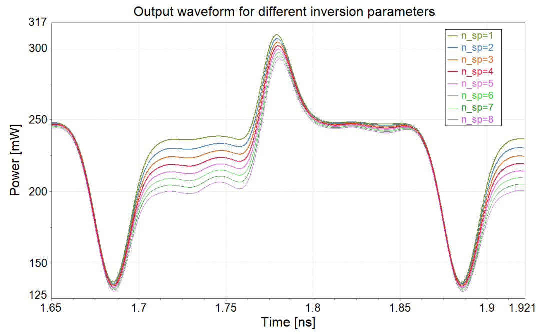

Figura 2.10. Influence of amplified spontaneous emission for $I_{SOA} = 350\,\mathrm{mA}$.

When n_{sp} increases higher optical energy is localised in the SOA, leading to stronger gain saturation. As expected, what is obtained from this phenomenon is a reduction of the gain, and then of the output intensity. This effect can be anyway only slightly noticed in figure 2.9, also for the highest, and quite unrealistic, values of n_{sp}.

On the contrary, when the injected current becomes much higher, as in figure 2.10, ASE starts to play an evident role. Here it can be noticed how changes in the inversion parameter lead to a clear alteration of the signal shape. It must anyway be remarked that this current value is associated with a gain $G \approx 30\,\mathrm{dB}$, which is extreme for the device under test.

What comes out then from these simulations is that ASE can have an important impact on the modelling of the device in some specific operating conditions. On the other hand this work focuses on moderate current injection levels only. The simulation of figure 2.9 is the main reference for such a condition and it proves how neglecting ASE is a reasonable choice.

Including the spontaneous emission contribution with a time dependent model would be, in any case, excessively computationally intensive for a successful DSP implementation. A viable way would be on the contrary to include ASE as an extra dependence on τ_c as demonstrated in [13]. With this approach the spontaneous lifetime would be evaluated as:

$$\tau_c = \frac{1}{A + BN + CN^2 + DN^2}, \tag{2.19}$$

where D is the extra coefficient related to ASE, which can be fitted from experiments.

Anyway in the following of this work ASE is simply neglected and care is taken to work in an operating point which satisfies this assumption.

Effect of spatial segmentation

The model under evaluation is based on input-output field relations in which the carrier density N is considered only as a spatially averaged value. In a real SOA, anyway, the power distribution in the device is not uniform, with higher values expected near the output facet, when signal amplification has been achieved travelling through the device. This effect translates in a non uniform carrier density over the z-axis which is not considered by the model.

In VPIphotonics it is possible to set the number of transmission line sections in which the device is divided. Tuning this parameter the results in figures 2.11 and 2.12 are obtained.

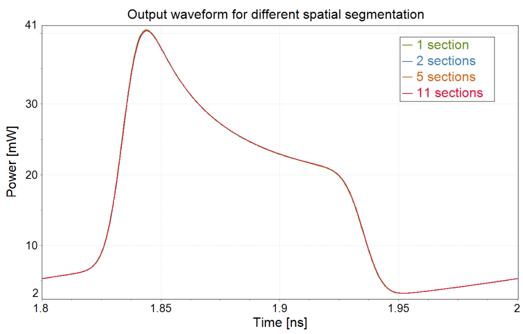

Figura 2.11. Effect of device segmentation on output waveform for $I_{SOA} = 50\,\mathrm{mA}$.

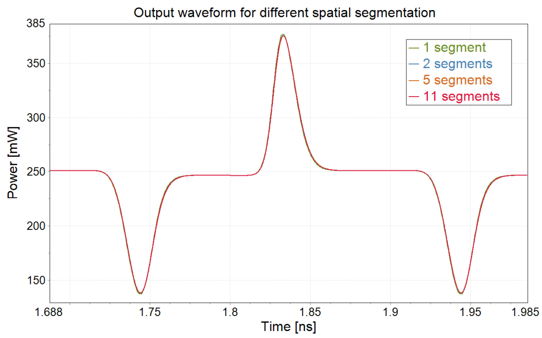

Figura 2.12. Effect of device segmentation on output waveform for $I_{SOA} = 350\,\mathrm{mA}$.

In these simulations the number of sections is swept from one to eleven. As it is possible to notice, in both cases the inclusion of longitudinal effects with a gradual increase in the accuracy does not show significant improvements in the results.

After this check it is then possible to state that a single section model preserves a very good accuracy. This allows the solution of only one differential equation for each time step increasing the efficiency of the model with respect to a spatially segmented one.

Effect of the time dependence of the spontaneous carrier lifetime

The most problematic approximation, already from a theoretical point of view, is setting the spontaneous lifetime to a value which is constant in time. To check the impact of this approximation the strategy is to simulate first a device with the standard values for A, B, C and then one in which B and C are set to zero but the linear recombination coefficient A' is such that:

$$\frac{1}{A'} = \frac{1}{A + BN_{ss} + CN_{ss}^2}. \tag{2.20}$$

In this way the same solution is given by the MATLAB model but in the first simulation VPIphotonics estimates the output with a time dependent lifetime model while in the second case this dependency is eliminated. The comparison of the results is shown in figure 2.13. Here a situation in which the output is strongly distorted, with $I_{SOA} = 350\,\mathrm{mA}$, is chosen to better appreciate the difference between the two cases.

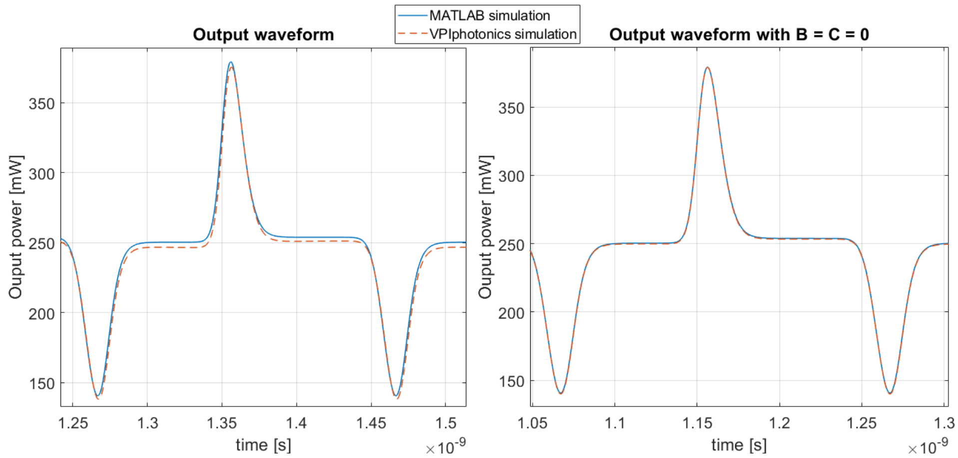

Figura 2.13. Influence of using a time independent lifetime value on the output waveform.

When the time dependency of τ_c is eliminated (plot on the right) the two models agree almost perfectly. On the contrary, if the time dependent model is used in VPIphotonics, the two model are still in good agreement but show some discrepancies.

The result of this analysis is that, as expected, imposing a constant lifetime is the most problematic approximation. In fact, while keeping the three approximations previously discussed, when getting rid of the time dependency of τ_c the two models agree almost perfectly, as shown in figure 2.13. This demonstrates that the weight of this approximation is by far the largest. This is anyway a limit of the model developed which must be accepted as it is: improving the estimation through an iterative recalculation of the lifetime at every time step would result in an excessively computationally intensive algorithm for being suitable to a DSP implementation.

2.3 Extension of the model for quantum wells based structures

2.3.1 Failure of the spatial averaged carrier density approximation

The spatial averaging performed while building the model (2.5) is an operation allowed by the linearity of the different terms with respect to $N(z)$. Unfortunately while the linear gain model of (1.5) is a good choice for simulation of bulk semiconductor structures, this proves to be not suitable for quantum wells (QW) based SOAs. In these devices the active layer is engineered through the use of multiple quantum wells and an adequate material gain model for such structures is based on a logarithmic relation that can be described as:

$$g = a' \ln\left(\frac{N}{N_{tr}}\right), \tag{2.21}$$

where a' does not correspond any more to the derivative of the gain with respect to the carrier density but is just a multiplicative factor.

In the rate equation (2.1) with linear gain model spatial averaging the carrier density is an allowed operation from a mathematical point of view. This since $\mathrm{E}[k_1 N + k_2] = k_1 \mathrm{E}[N] + k_2$, where k_1 and k_2 are constants and $\mathrm{E}[\cdot]$ represents the expected value. On the contrary, if (2.21) is used as the gain model, it is not possible to state that the average of the logarithm is the logarithm of the average. In mathematical terms this can be stated as:

$$\ln\left(\frac{\mathrm{E}[N]}{N_{tr}}\right) \neq \mathrm{E}\left[\ln\left(\frac{N}{N_{tr}}\right)\right]. \tag{2.22}$$

2.3.2 Equivalent linear gain model estimation

The redefinition of the model equations, starting from this new gain formula, is then not possible. The spatial averaging is in fact a fundamental operation in the model building process. A more viable approximated solution can be obtained keeping the linear model but with an adequate calculation of an equivalent differential gain a starting from a given factor a'.

The purpose of this is to keep the material gain fixed while changing the model. The equivalent a is then found, equalling the two gain models, as:

$$a = a' \frac{\ln\left(\frac{N}{N_{tr}}\right)}{N - N_{tr}}. \tag{2.23}$$

Now when τ_c is estimated, previously to the ODE solution, a can be substituted with (2.23) in which N is the unknown N_{ss}. In this way the correction for the logarithmic model acts on the estimated average carrier density value. Once N_{ss} is obtained, it is finally possible to estimate a again through (2.23) and this approximated parameter is then used for the usual ODE solution.

2.3.3 Validation of the logarithmic model

VPIphotonics is able to simulate devices with a logarithmic material gain model. The input signal is the OOK modulated one already used during the validation of the standard model and $a' = 1 \times 10^5\,\mathrm{m}^{-1}$ is set. Three simulations with injected currents of 35 mA, 50 mA and 350 mA are run to observe the agreement for increasing distortion levels. The obtained output waveforms are shown in figures 2.14, 2.15 and 2.16.

For low to moderate distortion levels, as in figures 2.14 and 2.15, the approximation returns results which show some discrepancies but still provide a good estimation. On the contrary, when a very strong distortion is present, as in figure 2.16, the model evidences its limits, returning an unreliable result.

What can be then extrapolated from these simulations is that this approximation proves useful if the distortion level is not excessively high, while it fails for very strong gain saturation levels. This behaviour is coherent with the theory behind the approximation: higher saturation implies stronger carrier density fluctuations, which reflects in a lower

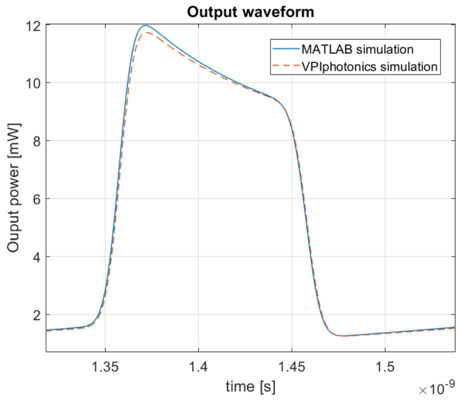

Figura 2.14. Output comparison for $I_{SOA} = 35\,\mathrm{mA}$ and $G \approx 10\,\mathrm{dB}$ with logarithmic gain model.

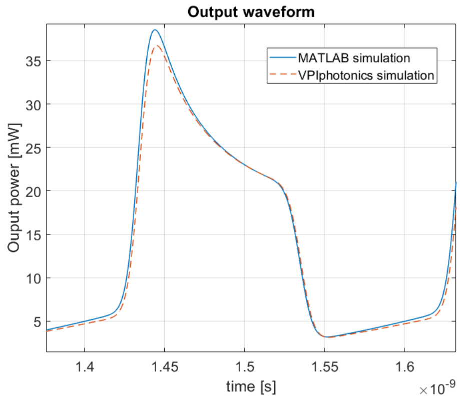

Figura 2.15. Output comparison for $I_{SOA} = 50\,\mathrm{mA}$ and $G \approx 14.5\,\mathrm{dB}$ with logarithmic gain model.

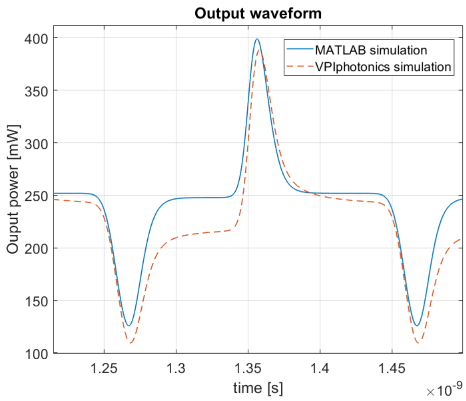

Figura 2.16. Output comparison for $I_{SOA} = 350\,\mathrm{mA}$ and $G \approx 27\,\mathrm{dB}$ with logarithmic gain model.

accuracy while evaluating the time independent N_{ss}. The equivalent parameter a is calculated starting from this value and a not reliable estimation influences the quality of the final solution. As already stated, anyway, very high distortion levels as in figure 2.16 are not commonly chosen operating points for a SOA in real systems. The behaviour of this extended model can then be considered satisfactory for most applications and has the advantage of not introducing additional algorithmic complexity.

Capitolo 3

Investigation of SOA induced distortion

Already in the previous chapters it has been possible to notice how the SOA induced intensity distortion varies depending on the device operating point. To investigate this dependence is crucial in order to be able to correctly compensate for SOA distortions using the model in its validity range. Another interesting point is to observe how the physical parameters of the device can influence the distortion introduced. Such a study is able to provide useful insights to guide the design of a SOA in order to obtain given specifications. In this chapter these different aspects are then going to be investigated.

3.1 Influence of the operating point on distortion

For a given SOA gain saturation is influenced by the bias point and the input signal. In particular, three factors have an influence on this aspect: the injected current, the input signal power and the modulation frequency. A short analysis is then performed for each of these parameters in this section.

3.1.1 Effect of the current injected in the SOA

The current injected in the device is the most easily tunable quantity to achieve a certain amplification. Increasing the gain, unfortunately, brings not only to higher gain but at the same time to a rapid deterioration of the signal due to distortion. Once again the reason for this phenomenon is the higher optical power in the device, which enhances carrier density fluctuations. For a given device it is then crucial to balance the obtained amplification with acceptable distortion when choosing the device operating point.

Studying the dependence of the gain on the injected current gives useful insights for this purpose. This relation is evaluated for the usual test device with the alternated OOK signal already used in chapter 2 as input. Through multiple simulations, with different current values, the results in figure 3.1 are obtained.

What comes out concerning the gain is that slightly above transparency the amplification grows exponentially with respect to the injected current to finally assume a linear dependence.

On the other hand it must be observed how the distortion grows together with the gain. In figure 3.2 I_{SOA} is swept from 30 mA to 100 mA. Already for this relatively low value it is clear how the signal shape deteriorates rapidly, not allowing to achieve arbitrarily high amplification in practical applications.

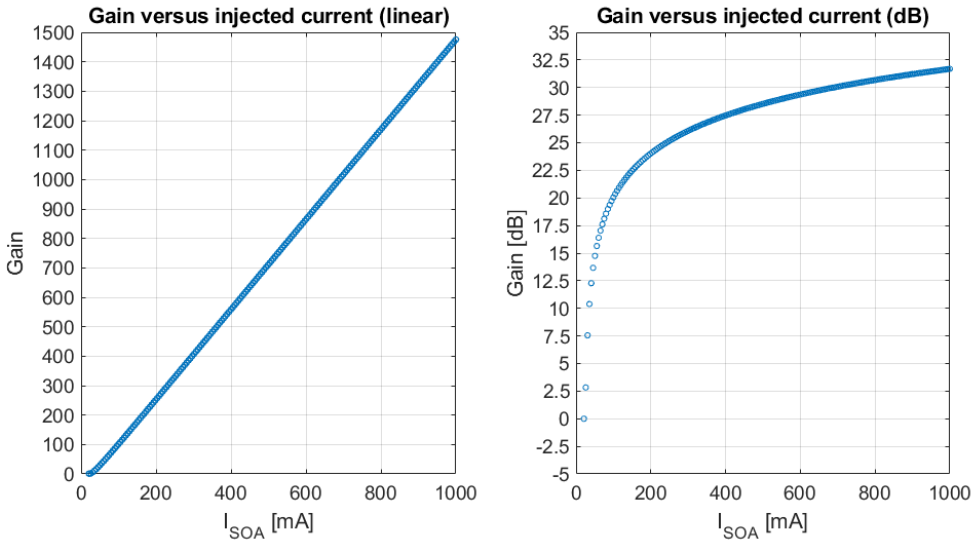

Figura 3.1. Gain versus current injected in the SOA for values from $I_{tr} = 21$ mA to 1 A.

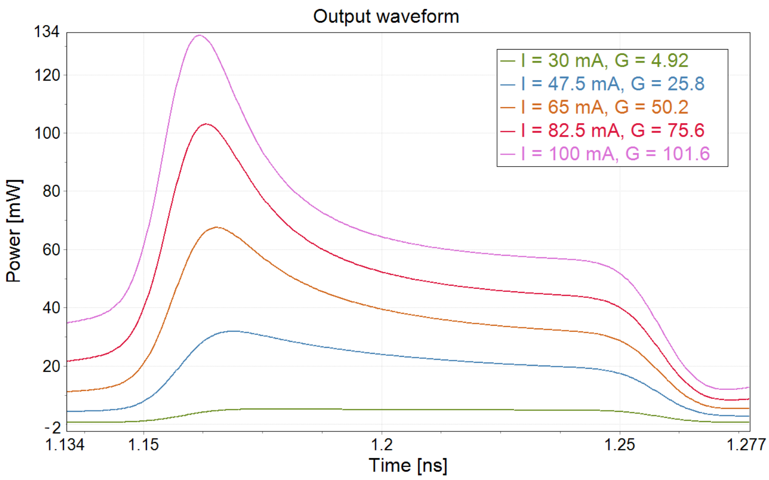

Figura 3.2. Output waveform for different injected current values.

3.1.2 Effect of input power

A stronger input signal tends to saturate more the gain. Intuitively if a given gain must be achieved both higher current is needed and more distortion is introduced. To observe this behaviour three simulations with different input powers are performed. In all of these the current is tuned in order to achieve a gain of approximatively 10 dB in order for the results to be comparable. The data and plots related to these analysis are reported in figures 3.3, 3.4 and 3.5.

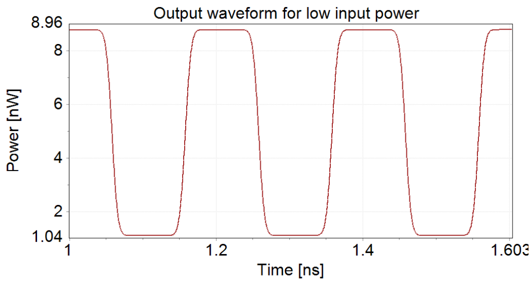

Figura 3.3. Output power for: $P_{in,0} = 110\,\text{pW}$, $P_{in,1} = 885\,\text{pW}$, $I_{SOA} = 27.8\,\text{mA}$.

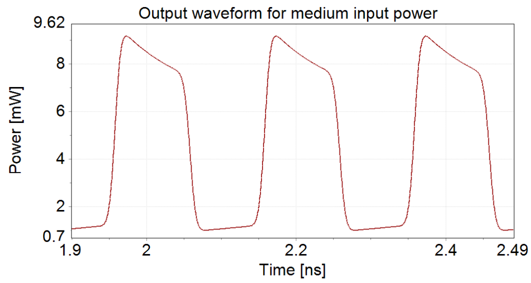

Figura 3.4. Output power for: $P_{in,0} = 110\,\mu\text{W}$, $P_{in,1} = 885\,\mu\text{W}$, $I_{SOA} = 33.3\,\text{mA}$.

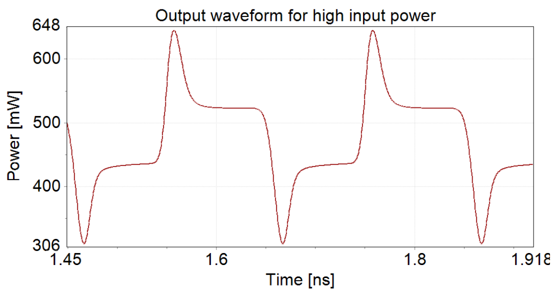

Figura 3.5. Output power for: $P_{in,0} = 11\,\text{mW}$, $P_{in,1} = 88.5\,\text{mW}$, $I_{SOA} = 570\,\text{mA}$.

The result of the simulations corroborates the hypothesis: for a given gain higher input power results in more current needed and stronger distortion.

3.1.3 Effect of modulation frequency

In section 1.2.3 the importance of the modulation frequency with respect to the lifetime has been already pointed out. It is anyway still interesting to estimate quantitatively how this factor influences the distortion for a given amplification. The imposed gain is still 10 dB and the modulation frequency is swept from 100 MHz to 100 GHz.

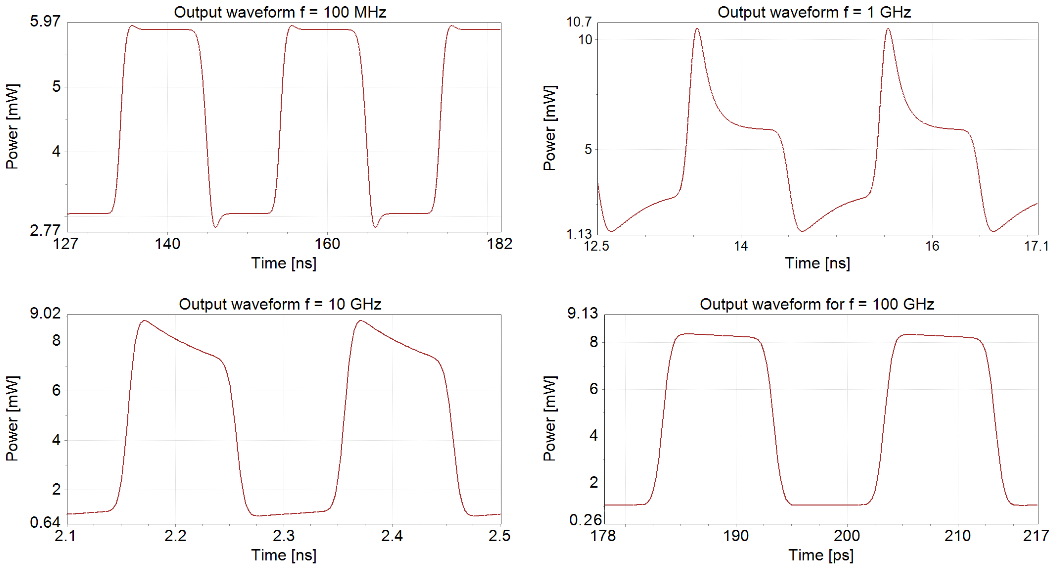

Figura 3.6. Simulated distorted waveforms for different modulation frequencies.

The simulation results, reported in figure 3.6, show how for $f_{mod} = 100\,\text{MHz}$ and $f_{mod} = 100\,\text{GHz}$ the distortion is not very evident. On the contrary a certain degradation of the signal shape is obtained when $f_{mod} = 10\,\text{GHz}$. What is anyway truly interesting is to observe how the situation is worsened in the most problematic frequency region, when $f_{mod} = 1\,\text{GHz} \approx 1/\tau_c$. A good piece of news is that communication systems work nowadays at much higher frequencies, achieving baud rates of the order of tenths of GBd/s. The last two plots in figure 3.6 are then more representative for practical applications.

3.2 Device parameters influence on SOA operation

3.2.1 Tunable parameters

The only way to reduce the amount of distortion for a given working point is to engineer the SOA in order to sustain higher power levels before saturating excessively the gain. At the same time it is important to maintain low the current needed: excessive current injection leads in fact to unreasonable power consumption and device heating. For a proper design the joint effect of the main tunable physical parameters of the device on these requirements must be then investigated:

- τ_c: the carrier lifetime is usually of the order of 1 ns but can be reduced introducing impurities in the active region, thus increasing scattering probability. Very strong reductions are anyway not recommended because of the negative impact of the process regarding device heating. Through this operation what is actually changed is the linear recombination parameter A, while B and C can be practically considered to remain constant.

Recalling that $P_{sat} = E_{sat}/\tau_c$, it is evident how lower values of τ_c lead to an improved saturation power.

- Γ: the confinement factor is mainly dependent on the active region's cross section σ and on the refractive index profile of the SOA. This last option in particular is the most effective way to tune this parameter. Reducing the transverse dimensions in fact results in linearly decreasing also the total volume, leading to no improvement for what concerns the saturation power.
- L: this parameter influences the gain achieved, which grows together with the length. At the same time anyway a larger value reflects in a bigger volume, probably resulting in higher injection current needed. Ideally this parameter has no direct influence on the saturation power.
- σ: the active region cross section influences both the confinement factor and the structure volume. It is hard to predict its impact on the device gain, while for what concerns the saturation power, on the contrary, it linearly increases with σ.

Other parameters such as the differential gain or the transparency carrier density are not easy to tune and so are taken as fixed values in this analysis.

From these short descriptions it can be noticed how the different parameters are strongly interconnected and it is not intuitive how to tune them in order to obtain given performance. In the next section then a numerical study is performed to understand which results are achievable and how the device must be engineered in order to provide them.

3.2.2 Numerical study of possible SOA operating region

To find which values of saturation power are achievable in relation to a certain input current the four parameters described in the previous section are swept in a realistic range. For every set of values simulations through the time efficient model developed are performed. In each of these simulations I_{SOA} is adaptively swept until obtaining a fixed gain of approximatively 10 dB. Every parameter is swept in twelve linearly spaced points, for a total of 20736 operating condition analysed. The parameter ranges used are:

- $A \in [1 \times 10^9\ ;\ 1 \times 10^{10}]\ \mathrm{s}^{-1}$
- $\sigma \in [0.02\ ;\ 0.4]\ \mu\mathrm{m}^2$
- $L \in [200\ ;\ 1000]\ \mu\mathrm{m}$
- $\Gamma \in [0.02\ ;\ 0.5]$

An automatic script is coded in MATLAB to perform this analysis, which would be not feasible if performed manually with a high number of points. Sweeping on such large ranges of values it is anyway not trivial, since the current needed can vary of several orders of magnitude through different simulations. A first problem to avoid is then the excessive increase of the simulation time. Using a small enough fixed current step in such a large range is unacceptably inefficient, an adaptive partitioning is then introduced. Another major issue is related to the exponential dependence of the gain on the current: values of I_{SOA} which are required for some structures can in fact provide numerically infinite results for others. Redefinition of the simulation range must be performed in this case.

In figure 3.7 the full flow diagram of this automatic routine is reported to show exactly how these problem are handled.

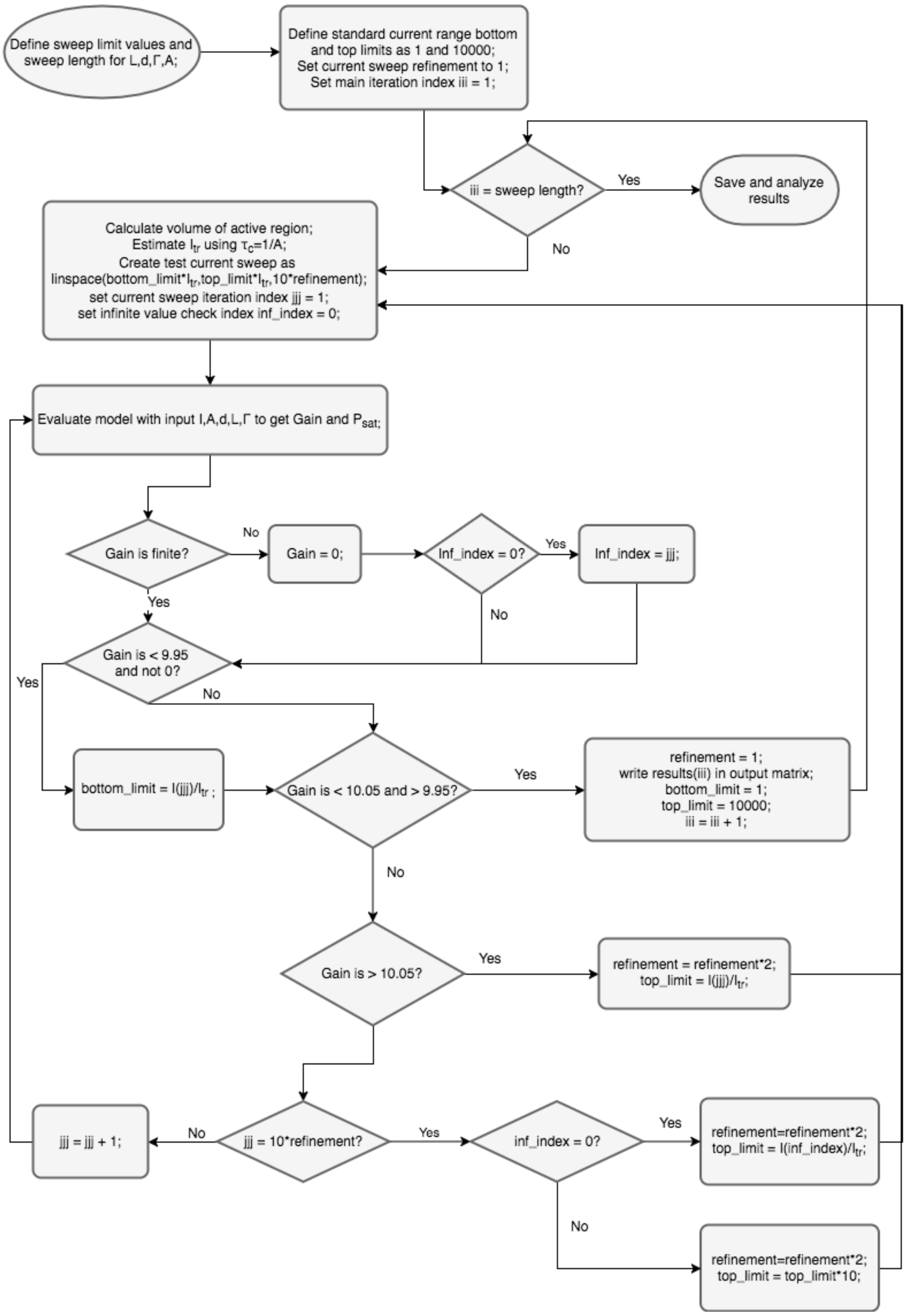

Figura 3.7. Flow diagram of the automatic parametric sweep.

The results given by this analysis are shown in figure 3.8. As a reference the test device used until now is characterized by a saturation power $P_{sat} = 0.97$ dBm and needs $I_{SOA} = 28.5$ mA to achieve a gain of 10 dB. It is then possible to appreciate how with a better choice of the device parameters for the same current $P_{sat} \approx 9$ dBm can be obtained, leading to a considerable reduction of the distortion. It is also possible to observe how reaching much higher P_{sat} forces to increase the current more and more to keep the gain constant. The analysis then proves that an ideal parameter choice does not exist. The device must be engineered accordingly with its specific application for optimisation purposes.

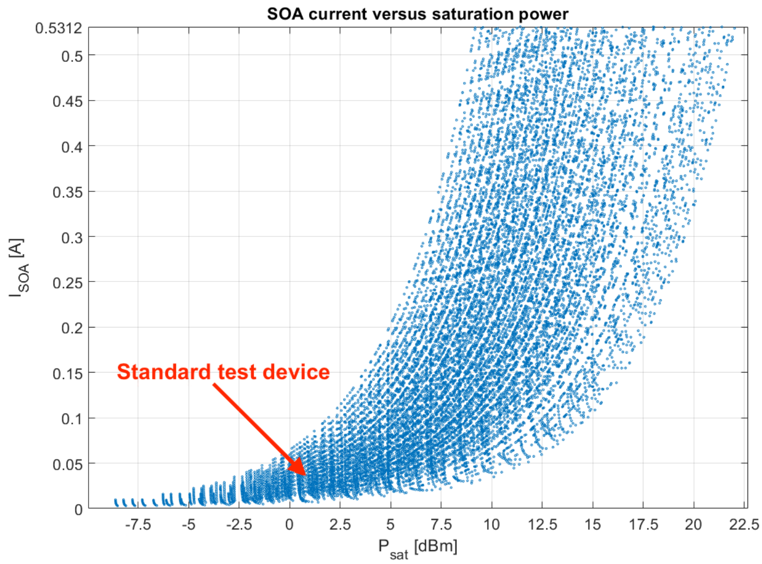

Figura 3.8. Injected current needed versus saturation power for obtaining a gain of 10 dB with different device parameters.

3.2.3 Comparison between standard test device and optimised one

The device cited in the previous section, which is able to provide a 10 dB gain together with $P_{sat} = 9$ dBm for $I_{SOA} = 28.5$ mA is characterised by the following parameters:

$$A = 1 \times 10^9\,\mathrm{s}^{-1}\ ,\ L = 200\,\mu\mathrm{m}\ ,\ \sigma = 0.04\,\mu\mathrm{m}\ ,\ \Gamma = 0.02\ . \qquad (3.1)$$

High saturation power devices are usually characterized by very low confinement factors [14], as in this case. The reduction of the volume with respect to the standard device keeps anyway the needed total current injected low also with a reduced Γ which is decreasing the gain. If the usual 10 GHz OOK test signal is given as input in VPI to the test SOA used until now and to this optimised device the output shown in figure 3.9 is obtained.

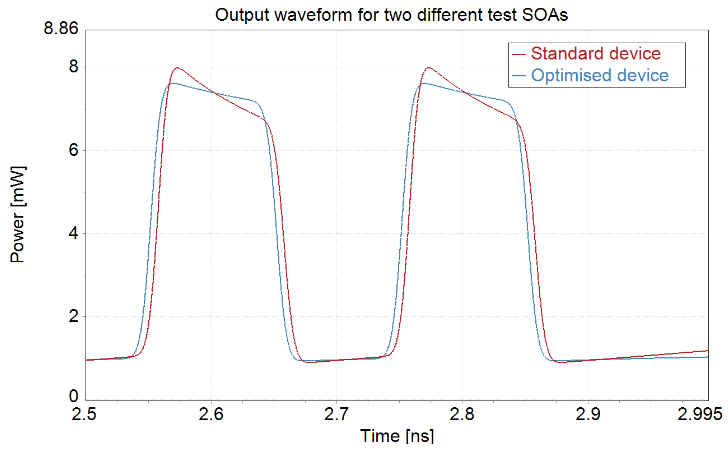

Figura 3.9. Output signals for standard device and optimised one with higher saturation power.

It is easy to notice how a more careful choice of the device parameters led to a reduction of the signal distortion for the same output power and without the need of increasing the injected current.

3.3 Effects of distortion on QAM constellation

Until now gain saturation has been observed looking at the distorted output power but no quantitative results has been given for what concerns the phase modulation. It is then time to look at both intensity and phase distortion by observing the effect of the SOA on the output constellation of a QAM input signal. In this section the VPIphotonics based setup used to perform this operation is presented, together with the obtained results.

3.3.1 Simulation setup

To plot the constellation diagram and obtain an estimation of the SER VPIphotonics comes in aid with a built in M-QAM receiver. This module includes all the needed DSP operations, such as clock recovery and phase/gain unbalance correction. The SER calculation is by default performed through a probabilistic estimation based on considering the received samples to follow a Gaussian distribution. This method is very efficient for giving a good estimation with relatively few symbols [15] but it performs properly when noise is the main source of error. In this case, in which a strongly non linear phenomenon such as SOA distortion is of interest, the Gaussian method may lead to severe underestimation of the SER [16]. A Monte Carlo method is then preferred also if leading to considerably longer simulation time for obtaining reliable results.

For what concerns the M-QAM transmitter the laser power is set in order to have an output signal with average power $P_{in,av} \approx -8.5$ dBm, similar to the one of the OOK test input used until now. Pulse shaping is for the moment not performed realistically: the transmitter's low pass filter is set to have a cut-off frequency of ten times the baud rate to achieve an almost ideal modulated output. The modulation frequency is set to

f_{mod} = 32 GBd/s and the modulation order to M=16. The simulation bench is shown in figure 3.10.

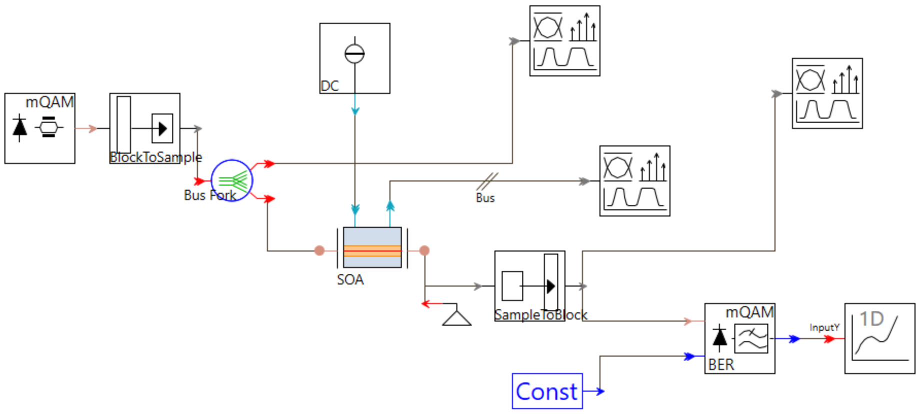

Figura 3.10. Simulation bench for constellation plot and SER estimation of QAM signal.

3.3.2 Effect of SOA distortion on the received constellation

A current I_{SOA} = 50 mA is applied to the usual test device and for the moment the linewidth enhancement factor is set to $\alpha = 0$. This allows to observe the effect of intensity distortion alone on the constellation. The result is shown in figure 3.11. For this simulation the gain is $G = 19.35$ dB and the estimated SER is 0.16%, already too high for practical applications.

Some interesting remarks can be made looking at this constellation: first of all the points are distributed over radial lines since $\alpha = 0$ and then only the module is influenced by the distortion. The outer points on the I-Q planes are harder to reach because of gain compression while on the contrary the inner points are over-amplified of a random amount which depends on the signal pattern.

When Self Phase Modulation (SPM) is included, setting $\alpha = 4$ and keeping all the other parameters constant, the constellation changes to what is shown in figure 3.12.

The effect of SPM is to impose a pattern dependent phase shift. This behaviour is clearly shown in the plot, where points with similar modulus are randomly phase and gain shifted, forming elliptically distributed tails on the I-Q plane. With the inclusion of this effect the SER is increased to 33%, making impossible to use such a device in this operating point without introducing any distortion compensation method.

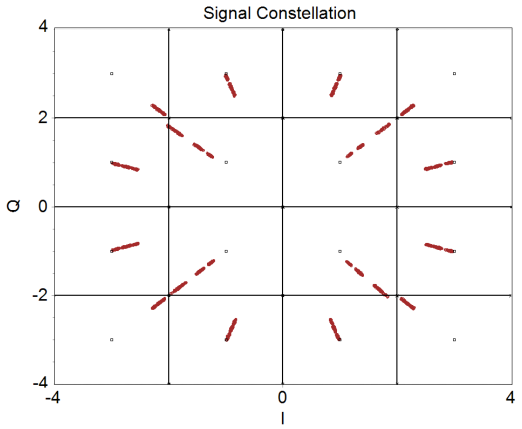

Figura 3.11. Output constellation when SPM is not taken into account.

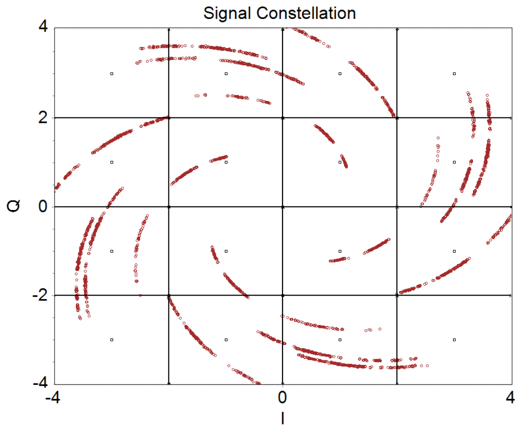

Figura 3.12. Output constellation when SPM is taken into account.

Capitolo 4

Non linear distortion compensation

As observed in chapter 3, in many situations QAM signals can not be amplified through a SOA and then directly being received because an unreasonable BER would be obtained. If this is the case methods must be developed for reducing the amount of distortion and decrease the BER. A non linear compensation method, based on the model previously derived in chapter 2, is then developed and tested. The idea behind this method is to invert the model in such a way to recover the transmitted waveform having knowledge about the received signal only. In the following of this chapter the model is inverted, its computational complexity discussed and the compensation is evaluated with the gradual inclusion of non idealities apt to simulate operation in a realistic environment. Finally the method is applied, with the needed modifications, also at the transmitter stage in a pre-compensation scheme and a comparison with the post-compensation method is performed.

4.1 Derivation and implementation of the non linear compensation

4.1.1 Theoretical derivation

Exploiting (2.13) it is possible to write the power at the SOA input $P_{in,SOA}$ as a function of h and the SOA output $P_{out,SOA}$:

$$P_{in,SOA} = \frac{P_{out,SOA}}{\mathrm{e}^h}. \tag{4.1}$$

Performing this substitution in (2.12) an equation describing the SOA operation which is only dependent on information provided by the SOA output is obtained:

$$\frac{dh}{dt} = \frac{g_0 L - h}{\tau_c} - \frac{P_{out}}{\mathrm{e}^h} \cdot \frac{\mathrm{e}^h - 1}{E_{sat}}. \tag{4.2}$$

Once at a certain time instant $h(t)$ is numerically obtained from (4.2) it is possible to evaluate the compensated output power and phase as:

$$P_{comp} = \frac{P_{out,SOA}}{\mathrm{e}^h} \quad , \quad \phi_{comp} = \phi_{out,SOA} + \frac{1}{2}\alpha h. \tag{4.3}$$

4.1.2 Numerical implementation and algorithmic complexity

To numerically implement the ODE (4.2) both a 4th order Runge-Kutta method and a simpler explicit Euler's method are coded in MATLAB. These two have opposite performance regarding execution time and accuracy: loading the same dataset in MATLAB, Euler's method proves to reduce the execution time of a factor of two; on the other hand Runge-Kutta method provides slightly better compensation, leading to a reduced BER. It must be anyway noticed that this reduction is, in most cases, lower than a factor two. The choice of the numerical implementation must then be performed depending which one between speed and accuracy is crucial for a given application. In the simulations performed in the following the compensation improvement is favoured over speed requirements and Runge-Kutta method is then used.

If Euler's method is chosen the steps performed to evaluate $h_i = h(t_i)$ at every time step t_i are:

$$\left.\frac{dh}{dt}\right|_i = \frac{-P_{out,SOA}(t_i)}{E_{sat}} + \frac{P_{out,SOA}(t_i)}{E_{sat}\mathrm{e}^{h_i}} + \frac{g_0 L}{\tau_c} - \frac{h_i}{\tau_c}, \tag{4.4}$$

$$h_{i+1} = h_i + \left.\frac{dh}{dt}\right|_i \cdot \Delta t. \tag{4.5}$$

With 4th order Runge-Kutta method the numerical implementations is instead as follows:

$$K_{1,i} = \frac{-P_{out,SOA}(t_i)}{E_{sat}} + \frac{P_{out,SOA}(t_i)}{E_{sat}\mathrm{e}^{h_i}} + \frac{g_0 L}{\tau_c} - \frac{h_i}{\tau_c}, \tag{4.6}$$

$$K_{2,i} = \frac{-P_{out,SOA}\left(t_i + \frac{\Delta t}{2}\right)}{E_{sat}} + \frac{P_{out,SOA}\left(t_i + \frac{\Delta t}{2}\right)}{E_{sat}\mathrm{e}^{h_i + \frac{1}{2}K_{1,i}\Delta t}} + \frac{g_0 L}{\tau_c} - \frac{h_i + \frac{1}{2}K_{1,i}\Delta t}{\tau_c}, \tag{4.7}$$

$$K_{3,i} = \frac{-P_{out,SOA}\left(t_i + \frac{\Delta t}{2}\right)}{E_{sat}} + \frac{P_{out,SOA}\left(t_i + \frac{\Delta t}{2}\right)}{E_{sat}\mathrm{e}^{h_i + \frac{1}{2}K_{2,i}\Delta t}} + \frac{g_0 L}{\tau_c} - \frac{h_i + \frac{1}{2}K_{2,i}\Delta t}{\tau_c}, \tag{4.8}$$

$$K_{4,i} = \frac{-P_{out,SOA}\left(t_i + \Delta t\right)}{E_{sat}} + \frac{P_{out,SOA}\left(t_i + \Delta t\right)}{E_{sat}\mathrm{e}^{h_i + K_{3,i}\Delta t}} + \frac{g_0 L}{\tau_c} - \frac{h_i + K_{3,i}\Delta t}{\tau_c}, \tag{4.9}$$

$$h_{i+1} = h_i + \frac{1}{6}\left(K_{1,i} + 2K_{2,i} + 2K_{3,i} + K_{4,i}\right) \cdot \Delta t, \tag{4.10}$$

where $\Delta t = (t_{i+1} - t_i)$.

With both methods a reduced number of floating point operations are performed. No iterations are needed and complex functions such as exponentials can be implemented through the use of a Look Up Table (LUT). The most important feature of the algorithm is anyway that only three parameters are needed: E_{sat}, τ_c and $g_0 L$. These can be estimated through a training sequence and their reduced number reflects in a very efficient estimation operation. All these features make the model very promising for a successful DSP implementation.

4.2 Compensation performance evaluation

The compensation method developed and coded in MATLAB is now introduced in a co-simulation environment in VPIphotonics. In this way the commercial software manages modulation, SOA modelling and SER estimation while the SOA output is manipulated through the coded MATLAB function implementing the compensation method.

The test signal chosen for this evaluation is 64-QAM, with $P_{in,av} = -10$ dBm, a baud rate of 32 GBd/s and a simulated gain of $G = 10.2$ dB, obtained injecting a current $I_{SOA} = 28.5$ mA. These parameters represent a realistic challenging situation for next generation optical transceivers and a good test bench for the compensation method.

First an almost ideal simulation is carried out. The input signal is characterised by unrealistically sharp edges (no pulse shaping), the OSNR after the SOA is set to 100 dB and 24 samples per symbol are provided to the compensation routine. The constellations obtained before and after applying the compensation method are shown in figure 4.1.

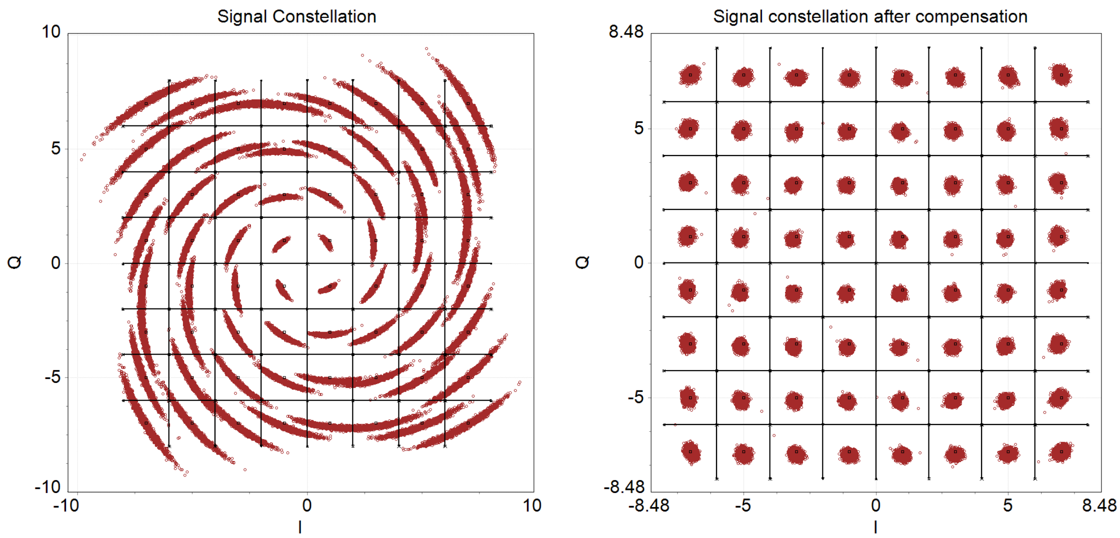

Figura 4.1. Received signal constellation before and after compensation.

With the proposed post-processing the SER is reduced from 0.07 to 8×10^{-5}. An improvement of three orders of magnitude which shows the potentialities of the method.

4.2.1 Inclusion of bandwidth efficient pulse shaping

In real applications the bandwidth of the transmitted signal must be limited through pulse shaping. This operation is needed in order for the signal to be properly treated by optoelectronic components and to avoid occupying a too wide band in the communication channel. Pulse shaping can be performed through low-pass filtering at the transmitter stage and a common choice for this purpose is represented by the use of raised cosine shaped filters. The response in time and frequency domain of this kind of filters is reported in figure 4.2. The impulse response of such a filter is characterized by being exactly zero in the time instants $t_i = kT$, where $k \in \mathbb{Z}^0$ and T is the symbol period. This property ideally eliminates Inter Symbol Interference (ISI) if the signal frequency is perfectly constant over time. Unfortunately a SOA introduces chirp in the signal, leading to still have ISI up to some extent. Because of this non ideality an important factor to tune is the filter roll-off β: this parameter can assume values comprised between zero and one and the effect of its reduction on the impulse response is to cause higher secondary oscillations. Frequency errors can lead then to altered data passed to the compensation routine, since the raised cosine function becomes considerably different from zero in several time points $t_i = k\Delta T$. On the other side, if one looks at the frequency response of the filter, it is easy to notice how a larger roll-off gives an unwanted increased bandwidth. This factor must be then tuned in order to both keep the compensation effective and to reduce the bandwidth to acceptable values. For this purpose $\beta = 0.8$ proved to be a good compromise through many simulations. With such value no evident worsening on the compensation effect is observed and this it is then the value of choice for the following of the analysis.

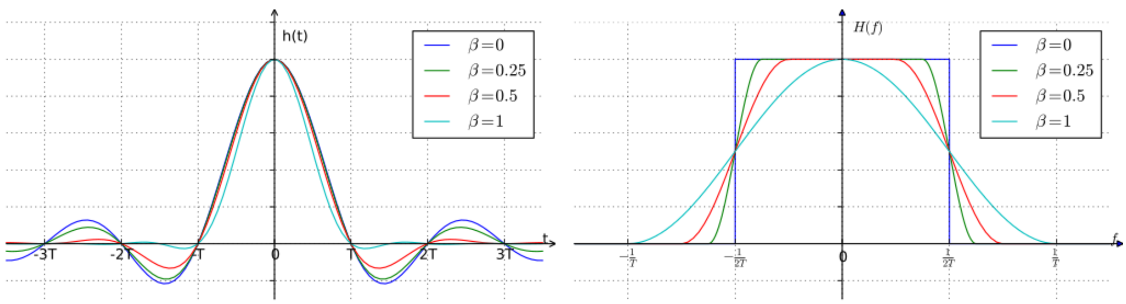

Figura 4.2. Impulse response (left) and frequency response (right) of a raised cosine filter for different roll-off factors

To show the effect of pulse shaping in figure 4.3 the output waveform and spectrum of a 16-QAM, 25 GHz transmitter are shown with and without introducing the raised cosine filter. In the almost ideal case, where the filter has a cut-off frequency of 500 GHz, an almost perfect square digital signal is obtained. On the contrary introducing the raised cosine filter with $\beta = 0.8$ leads to smoothing and attenuating the waveform, but also to a reduced bandwidth.

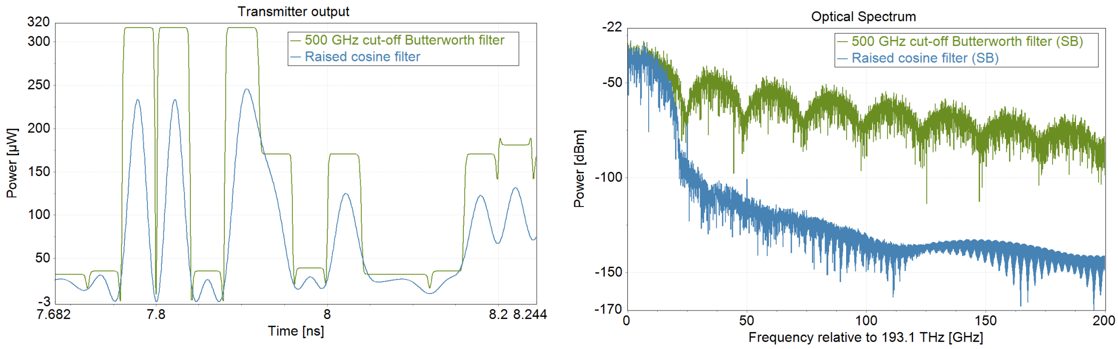

Figura 4.3. Received signal constellation before and after compensation.

4.2.2 Reduction of sampling rate to realistic values and introduction of additive noise

To test the compensation method in a realistic situation, two major non idealities must be taken into account: having a limited sampling rate and additive noise.

For what concerns the sampling rate, working on bit rates in the Gbit/s range, characterizing modern communication system, the current ADC technology prevents to achieve more than two to three samples per symbol. To emulate this condition in the simulation environment then the signal generated by VPIphotonics is down-sampled before being processed by the MATLAB routine. Working on a reduced set of samples is expected to affect negatively the accuracy of the SOA model, thus leading to a worsened compensation.

Regarding noise it is well known that this plays a major role in any communication system. Noise is introduced on the signal at every stage and a full analysis of the processes characterizing it is not trivial. A significant figure of merit that can be anyway used to take its effect into account is the Optical Signal to Noise Ratio (OSNR). This is defined as the power ratio between optical signal and noise. A built-in block of VPIphotonics, able to impose a given OSNR, can be introduced after the SOA output and before the compensation for including this effect in the simulation bench. The result of adding noise on the input of the compensation routine is to randomly change the sampled values from the ideal ones. What is worse is that this detrimental effect can couple together with the reduced sampling rate, leading to a reconstructed waveform much different from the real one.

To analyse the impact of these two non idealities and their interaction a simulation is then performed. The input signal and simulated gain are the same already used in the previous section. The OSNR is swept between 20 dB and 60 dB while the number of samples from 1.2 to 24 per symbol. The results of this parametric sweep is reported in figure 4.4.

The expected detrimental effects are confirmed by the simulation, which gives some interesting insights on the applicability of the compensation: reducing the sampling rate does not provide a dramatic worsening of the performance until values below 2 samples per symbol are reached; the OSNR, on the contrary, plays a major role and for values

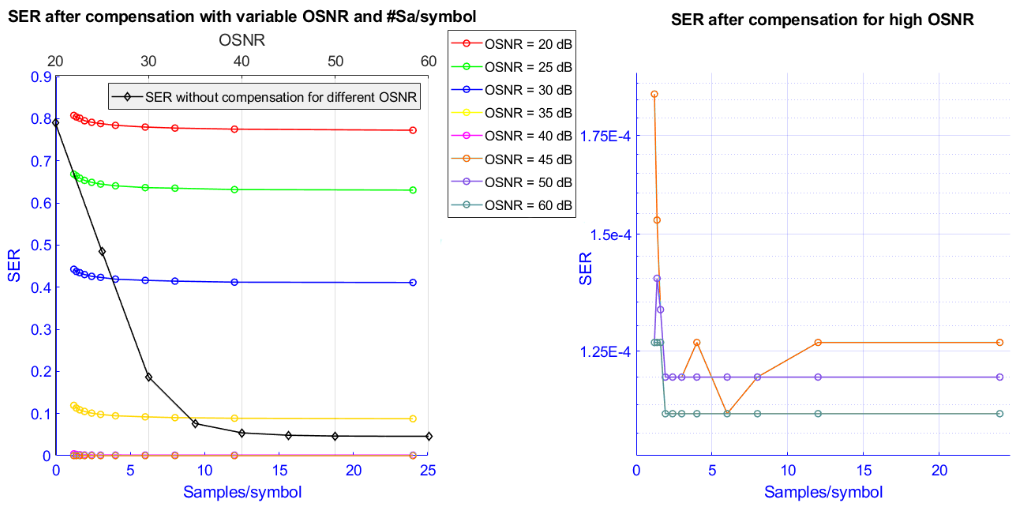

Figura 4.4. Simulation results for variable sampling rate and OSNR. On the left the SER after compensation is plotted for every simulation step together with the non compensated SER versus OSNR (black curve). On the right a zoomed plot of the obtained SER for the highest OSNR values is shown.

lower than 40 dB the obtained SER is too high for practical applications. In this situation, moreover, the compensation actually deteriorates the SER because of unreliable signal sampling.

4.3 Non linear pre-compensation

Post-compensation, implemented as supplementary DSP in the receiver, is the most straightforward way to apply the numerical method developed. On the other hand this approach has shown severe limitations with realistic OSNR values and pre-compensation could offer many advantages: it allows embedding the correction in the transmitter stage, thus making possible to use any receiver which does not implement SOA compensation; it is much less sensitive to noise, since the signal is processed before being sent on the optical link. These advantages come at the cost of introducing DSP in the transmitter, increasing power consumption and complexity, but can be very interesting in several situations in which noise represents the main issue or in which it is not possible to operate on all the receivers of the system.

4.3.1 Numerical method adaptation to pre-processing

While developing the post-compensation the problem was to find $h(t)$ characterising distortion in order to reconstruct the input starting from the output. The new problem statement is to find both $h(t)$ and a time dependent function $f(t)$ for which the input signal shape will be recovered with gain G after travelling through the SOA. Mathematically this translates in the condition:

$$P_{out}(t) = GP_{in}(t) = P_{in}(t) \cdot f(t) \cdot \mathrm{e}^{h(t, P_{in} \cdot f)}. \tag{4.11}$$

From (4.11) it is evident that:

$$f(t) = \frac{G}{\mathrm{e}^{h(t)}}. \tag{4.12}$$

Then the compensation can be implemented through Euler's method simply as follow:

$$\left.\frac{dh}{dt}\right|_i = \frac{g_0 L - h_i}{\tau_c} - \frac{P_{in} f_i}{E_{sat}} \left(\mathrm{e}^{h_i} - 1\right) \tag{4.13}$$

$$h_{i+1} = h_i + \left.\frac{dh}{dt}\right|_i \cdot \Delta t \tag{4.14}$$

$$f_{i+1} = \frac{G}{\mathrm{e}^{h_{i+1}}} \tag{4.15}$$

$$P_{in,SOA,i+1} = P_{in,i+1} f_{i+1} \quad , \quad \phi_{in,SOA,i+1} = \phi_{in,i+1} - \frac{1}{2}\alpha h_{i+1} \tag{4.16}$$

where $P_{in,SOA}$ and $\phi_{in,SOA}$ are the power and phase given as output from the model and represent the input of the SOA, not to be confused with P_{in} and ϕ_{in} which are the output of the transmitter.

With respect to post-compensation it is possible to notice the presence of the extra equation (4.15). The new variable $f(t)$ is given a starting condition $f_1 = G/\mathrm{e}^{h_1}$ and in the ODE $P_{in} f$ is now the input power used for the estimation of h.

For what concerns the lifetime estimation, having no a priori information about the SOA output or input, a feedback mechanism must be introduced. The pre-distortion is in fact dependent from the SOA input power, which is in turn influenced by the compensation, thus creating a closed loop. This feedback can be numerically implemented as an iteration of the full model with initial condition $P_{in,SOA} = P_{in}$. It is then sufficient to run again the routine with the updated $P_{in,SOA,j} = P_{in} f_j$ until convergence is obtained. It is important to notice that while this process slows down the simulation it does not affect a real implementation. In this case it is sufficient to use a power meter in feedback from the output of the SOA to the DSP for a one-time device characterisation.

4.3.2 Pre-compensation performance evaluation

After having changed the compensation routine a new simulation bench is created in VPIphotonics. A meaningful comparison with the simulation performed with post-compensation is desired and then the same transmitter is used, two samples per symbol are given to the compensation routine and the gain is set to 10 dB.

While finding the SOA current needed to achieve this amplification interesting insights on this compensation method can be obtained. In figure 4.5 the gain and the SOA average input power versus the injected current are shown, here I_{SOA} is swept starting from the transparency value. Looking at the graph, before a certain point the obtained gain shows to be higher than the imposed one. This apparently counter-intuitive solution is based on the fact that for this values the SOA has no gain and the pre-compensation leads to an increase in the average power from the transmitter output value. This is numerically a valid solution but it is of no practical interest since it just moves the problem of optical amplification from the SOA to the previous stage. In the following flat area of the graph is instead found the working region of the compensation method: after a certain value $I_{SOA,min} = 28.5\,\text{mA}$ the SOA input is characterised by lower average power than the transmitter output and is then over-amplified by the SOA to get the desired $P_{out,SOA}/P_{in}$ gain. Values up to $I_{SOA,max} = 31.5\,\text{mA}$ are all possible solutions with fixed gain. Inside this range increasing the current leads to a smaller input in the SOA, subject then to higher amplification. The resulting output power is anyway the same and the choice of the bias point is then freely tunable in this range. A reasonable choice can be to pick the lowest current possible to reduce heating and power consumption. In the final part of the graph, for current values over $I_{SOA,max}$, the input signal becomes too small and the SOA is not able any more to provide the needed over-amplification.

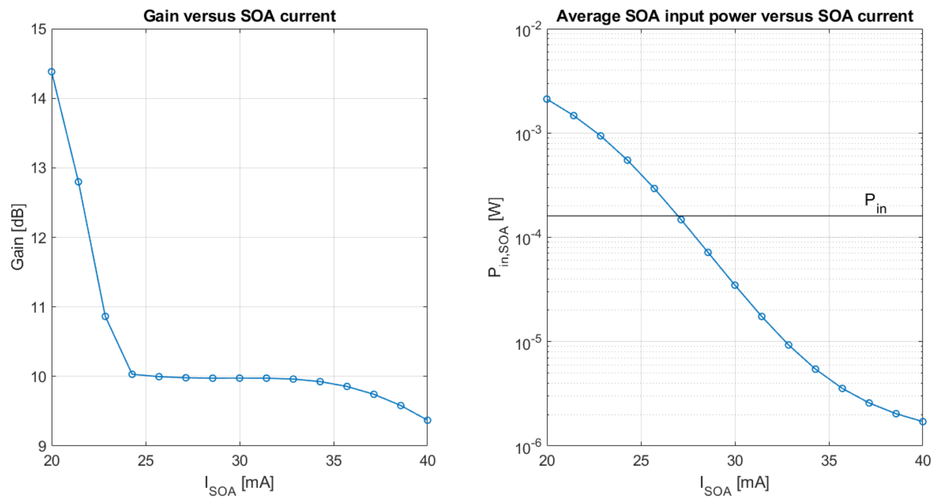

Figura 4.5. Gain and SOA input average power for different injected currents.

The signal constellations, with and without introducing pre-compensation, are shown in figure 4.6. The method proves to work very effectively: the SER is reduced from 6.6% to an estimated value of zero providing 2 samples per symbol to the routine. It must be anyway noted that this ideal value is the result of a Monte Carlo simulation with 10^5 test symbols. Statistically it is then possible to roughly estimate that the expected SER is lower than 1×10^{-5}. A non zero estimation has not been obtained since it would require an even higher number of symbols. Such a simulation would translate in an excessive computational time.

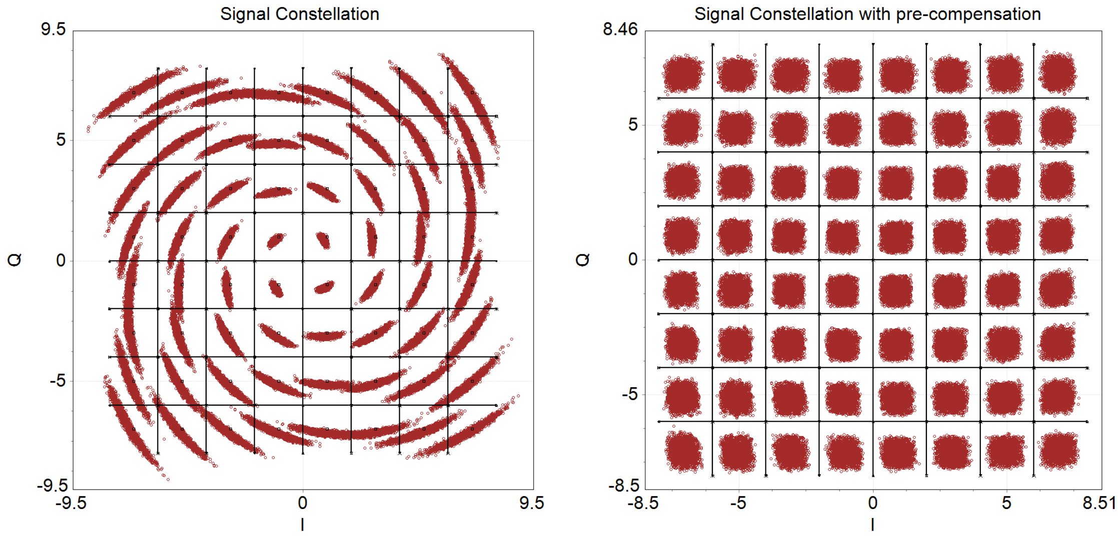

Figura 4.6. Signal constellation without (left) and with pre-compensation (right).

Capitolo 5

Non DSP based compensation methods

The method presented in chapter 4 proved to be effective but at the cost of additional DSP introduced in the system. It would be interesting to achieve compensation also without relying on DSP. For this purpose two different methods are developed and tested in this chapter: the first is based on linear filtering of the distortion while the other consists in driving the SOA with a fixed voltage, instead than through constant current injection.

5.1 Linear distortion filtering

5.1.1 Small signal input-output response derivation

A linear filter to attenuate the distortion can be obtained through a small signal analysis based on equations (2.12) and (2.13) around a certain bias point. This is of course a strong approximation since in reality the signals are not at all much smaller than the bias, but a compensation based on this idea is anyway expected to lead to a certain improvement in the output signal shape. The quantities in play under this assumption can be rewritten as

$$P_{out} = P_{out,0} + \Delta P_{out} \quad , \quad P_{in} = P_{in,0} + \Delta P_{in} \quad , \quad h = h_0 + \Delta h. \tag{5.1}$$

Then (2.13) becomes:

$$P_{out,0} + \Delta P_{out} = (P_{in,0} + \Delta P_{in}) \cdot \mathrm{e}^{h_0+\Delta h} = P_{in,0} \cdot \mathrm{e}^{h_0+\Delta h} + \Delta P_{in} \cdot \mathrm{e}^{h_0+\Delta h}. \tag{5.2}$$

The exponential term can be expanded to the second order $e^{\Delta h} \approx 1 + \Delta h + \frac{\Delta h^2}{2}$, $\Delta h \to 0$ and if the steady state condition $P_{out,0} = P_{in,0} \cdot \mathrm{e}^{h_0}$ is imposed it is possible to write:

$$\Delta P_{out} = P_{out,0} \cdot \Delta h + P_{out,0} \cdot \frac{\Delta h^2}{2} + \Delta P_{in} \cdot \mathrm{e}^{h_0} \left(1 + \Delta h + \frac{\Delta h^2}{2}\right). \tag{5.3}$$

At this point to find the small signal response $\Delta P_{out}/\Delta P_{in}$ it is needed to evaluate Δh. To find this term (2.12) must be linearised, assuming harmonic signals the equation becomes:

$$j\omega\Delta h\cdot \mathrm{e}^{j\omega t}=\frac{g_0L}{\tau_c}-\frac{h_0}{\tau_c}-\frac{\Delta h\cdot \mathrm{e}^{j\omega t}}{\tau_c}-\frac{P_{in,0}+\Delta P_{in}\cdot \mathrm{e}^{j\omega t}}{E_{sat}}\left(\mathrm{e}^{h_0}\left(1+\Delta h\cdot \mathrm{e}^{j\omega t}\right)-1\right). \quad (5.4)$$

Introducing the steady state condition:

$$\frac{g_0L-h_0}{\tau_c}-\frac{P_{in,0}}{E_{sat}}\left(\mathrm{e}^{h_0}-1\right)=0, \quad (5.5)$$

Δh is finally obtained as:

$$\Delta h=\frac{1-\mathrm{e}^{h_0}}{E_{sat}\left(j\omega+1/\tau_c+P_{out,0}/E_{sat}\right)}\cdot\Delta P_{in}. \quad (5.6)$$

Renaming A_1 the term $1/\tau_c + P_{out,0}/E_{sat}$ and substituting (5.6) in (5.3) the small signal response relating input and output power is finally found as:

$$\begin{aligned}\Delta P_{out}=\mathrm{e}^{h_0}&\left(1+\frac{P_{in,0}\left(1-\mathrm{e}^{h_0}\right)}{E_{sat}(j\omega+A_1)}\right)\Delta P_{in}+\\ +\,\mathrm{e}^{h_0}&\left(\frac{1-\mathrm{e}^{h_0}}{E_{sat}(j\omega+A_1)}+\frac{\left(1-\mathrm{e}^{h_0}\right)^2}{2\cdot E_{sat}^2(j\omega+A_1)^2}\right)\Delta P_{in}^2+\\ +&\,\frac{e^{h_0}\left(1-\mathrm{e}^{h_0}\right)^2}{2\cdot E_{sat}^2(j\omega+A_1)^2}\Delta P_{in}^3.\end{aligned} \quad (5.7)$$

The first term of the RHS of (5.7) is the term of interest for building the filter while the following terms represent second and third order intermodulation products.

5.1.2 Correction implementation and results

Once the theoretical equation is obtained it is possible to evaluate the linear frequency response for different bias points. Through this simulation the plot of figure 5.1 is obtained.

In all cases the gain increases for high frequencies and the response is of an high-pass type. For larger input average powers the achieved gain is obviously lower because of a stronger gain saturation. The cut-off frequency is also shifted to higher values when the input power increases.

The time-continuous filter transfer function is the inverse of the input-output linear response, that is:

$$\mathrm{TF}(j\omega)=\frac{1}{\mathrm{e}^{h_0}\left(1+\frac{P_{in,0}\left(1-\mathrm{e}^{h_0}\right)}{E_{sat}(j\omega+S)}\right)}. \quad (5.8)$$

Here $P_{in,0}e^{h_0}$ is taken as the average power of the SOA output and h_0 is evaluated through a numerical solution of the steady state equation (5.5). The resulting filter has then a low-pass response with cut-off frequency in the MHz to GHz range for the power levels analysed.

This filter shape is what makes this method not suitable for correcting amplitude modulated signals: a low-pass filtering at frequencies lower than f_{mod} results in cutting the modulation component together with the distortion. This phenomenon can be observed in figure 5.2, where the correction is simulated with the 10 GHz OOK signal already used in the previous chapters and $I_{SOA} = 50\,\mathrm{mA}$.

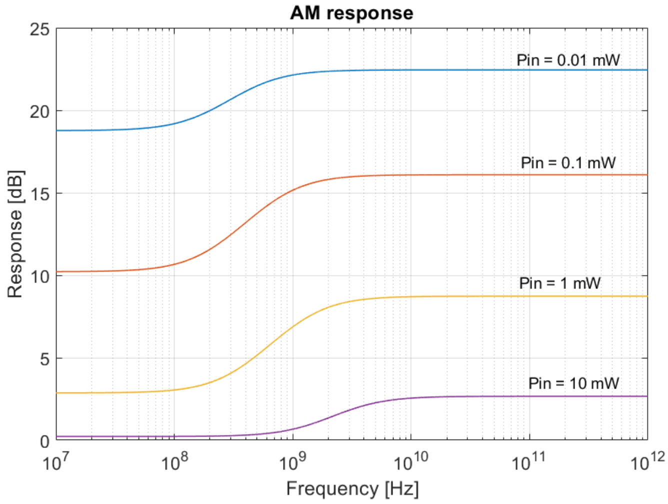

Figura 5.1. Input-output linear response for different SOA output power levels.

From the plots it can be appreciated how after the compensation the output signal shape is improved but at the cost of a dramatic reduction of the extinction ratio. This result is negatively influencing the BER obtained because of the reduction in the distance between different transmitted levels. This compensation method must be then unfortunately abandoned.

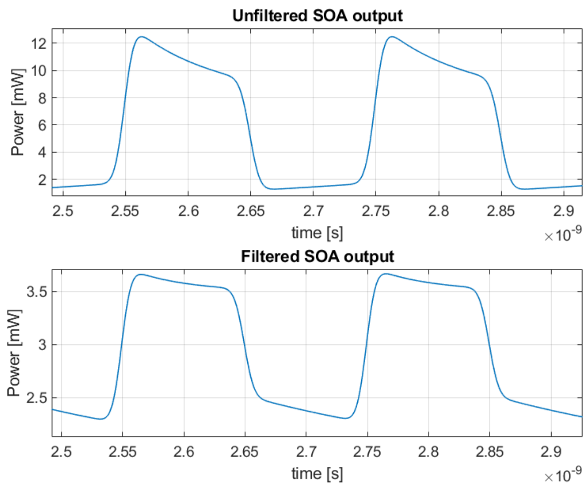

Figura 5.2. SOA output before and after compensation

5.2 SOA voltage driving

5.2.1 Equivalent circuit analysis

Until now the SOA has been biased through the injection of a constant current. This continuous introduction of carriers in the active region, together with the depletion due to stimulated recombination, is characterised by carrier density fluctuations. When this phenomenon takes place a time dependent shift of the quasi-Fermi levels in the semiconductor follows. A non-constant difference of potential at the SOA terminals can be then observed. On the contrary, if a constant voltage is applied to the device, it is ideally possible to prevent the quasi-Fermi levels to shift and then to avoid carrier density fluctuations while achieving optical gain.

In figure 5.3 the schematic representing the voltage generator and an equivalent circuit of the SOA is shown. This last can be modelled as an ideal diode with a series differential resistance R_d and a capacitor in parallel. C in the schematic is anyway a much bigger integrated capacitor, introduced to keep the potential difference more or less constant at the SOA terminals. Finally V_g is the bias voltage and R_g is the generator resistance, assumed to have the standard $50\,\Omega$ value.

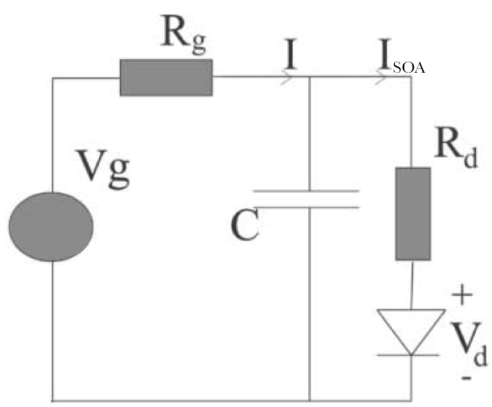

Figura 5.3. Equivalent circuit for a voltage driven SOA.

The main threat to this compensation method is represented by R_d. Also if the voltage drop on the capacitor is assumed constant still the difference of potential on the SOA fluctuates with amplitude $\Delta I_{SOA} R_d$. It is then necessary to numerically study the effect that R_d has on the compensation.

5.2.2 Model for the simulation of voltage driven SOA distortion

Starting from the model developed in chapter 2, the distortion of a SOA driven as in figure 5.3 can be simulated simply introducing another rate equation describing the charge on the capacitor [17]. The usual carrier rate equation to solve to find N in the SOA active region can be written as:

$$\frac{dN}{dt} = \frac{I_{SOA}(t)}{qV} - \left(AN + BN^2 + C_{auger}N^3\right) - \frac{\Gamma a(N - N_0)}{\hbar\omega_0 V}\int_0^L P_{in}\mathrm{e}^{\Gamma a(N-N_0)z}dz. \quad (5.9)$$

The now time dependent I_{SOA} can be found through circuital analysis as:

$$I_{SOA} = \frac{qQ_c - CV_d}{CR_d}, \quad (5.10)$$

where Q_c is the number of carrier in the capacitor and V_d is the voltage across the SOA. Q_c is obtained from the rate equation:

$$\frac{dQ_c}{dt} = \frac{V_g}{qR_g} - \frac{Q_c}{R_gC} - \frac{Q_c}{R_dC} + \frac{V_d}{qR_d}. \quad (5.11)$$

In this formula V_d is the potential energy difference between the quasi-Fermi levels divided by the elementary charge:

$$V_d = \frac{E_g + \Delta E_{fc} - \Delta E_{fv}}{q}. \quad (5.12)$$

Here ΔE_{fc} and ΔE_{fv} are the distances of the quasi-Fermi levels from the conduction and valence band edges and can be estimated through the following relations, known as Nilson formulae [12].

$$\Delta E_{fc} = k_BT\left[\ln\left(\frac{N}{N_c}\right) + \frac{N}{N_c}\left(64 + 0.05524\frac{N}{N_c}\left(64 + \sqrt{\frac{N}{N_c}}\right)\right)^{-\frac{1}{4}}\right], \quad (5.13)$$

$$\Delta E_{fv} = -k_BT\left[\ln\left(\frac{N}{N_v}\right) + \frac{N}{N_v}\left(64 + 0.05524\frac{N}{N_v}\left(64 + \sqrt{\frac{N}{N_v}}\right)\right)^{-\frac{1}{4}}\right], \quad (5.14)$$

where k_B is the Boltzmann constant, T is the absolute device temperature and N_c, N_v are the effective density of states respectively at the conduction and valence band edges. These last two factors are defined as:

$$N_c = 2\left(\frac{2\pi m_e^* k_BT}{h^2}\right)^{\frac{3}{2}} \quad , \quad N_v = 2\left(\frac{2\pi m_h^* k_BT}{h^2}\right)^{\frac{3}{2}}. \quad (5.15)$$

For evaluating these the effective mass of the electrons m_e^* is estimated as $m_e^* = 0.045m_0$, where m_0 is the rest mass of an electron. For what concerns the effective mass of holes instead $m_h^* = \left[(0.056m_0^{1.5}) + (0.46m_0^{1.5})\right]^{2/3}$ is used as an estimation to take into account both heavy and light holes.

Substituting all these definitions and finally solving (5.9) $N(t)$ is obtained and it is possible to calculate the output intensity as:

$$P_{out}(t) = P_{in}(t)\mathrm{e}^{\Gamma a(N(t)-N_{tr})L}. \quad (5.16)$$

5.2.3 Numerical results and comparison with constant current driving

The set of equations (5.9) - (5.16) is implemented in MATLAB and the 10 GHz OOK test signal often used throughout this work is once again chosen as the input for the simulation. Care must be taken in looping the model through different runs, with updated starting condition, until steady state is reached. This necessity is due to the RC constant of the system, which can become much longer than the signal period. For what concerns the circuital parameters $V_g = 4\,\mathrm{V}$ and $C = 100\,\mathrm{nF}$ are set.

Different test are performed with increasing values of the SOA series resistance from $R_{d,min} = 0.5\,\mathrm{m}\Omega$ to $R_{d,max} = 5\,\Omega$. The same simulation is also performed through current driving with $I_{SOA} = 49\,\mathrm{mA}$ to achieve the same gain of 15.5 dB obtained for $R_d = 5\,\Omega$. This last is chosen as the reference case both because it is the least ideal situation and the most realistic. A differential resistance below some ohms is practically very hard to achieve because of the need for excessive contact doping which then diffuses in the device, impacting on its operation.

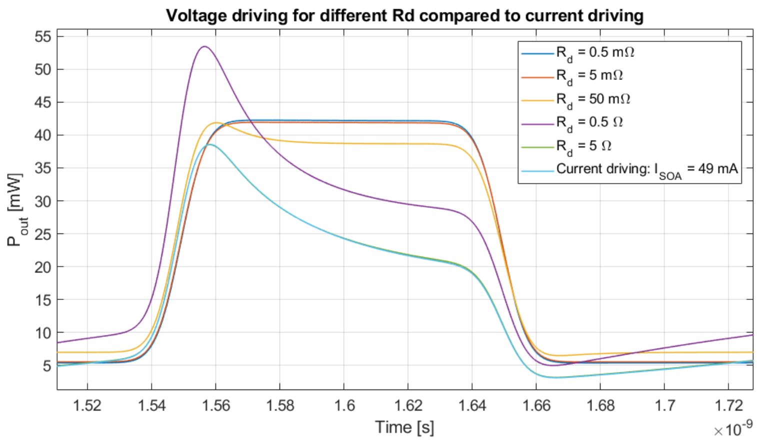

Figura 5.4. Distortion simulation results for different values of R_d and for current driving.

When the differential resistance is up to $5\,\mathrm{m}\Omega$ the distortion is almost perfectly corrected as expected from the theory. Unfortunately if R_d is increased to $50\,\mathrm{m}\Omega$ and $500\,\mathrm{m}\Omega$ the voltage drop on the resistance becomes considerable, introducing gain saturation in the SOA. Finally when $R_d = 5\,\Omega$ the result is almost exactly the same obtained with constant current driving.

This simulation then shows how theoretically this compensation method works perfectly and has the advantage of not requiring any data processing. On the other hand, to make the compensation effective, values of the SOA series resistance which are unrealistic with the current technology need to be achieved.

Capitolo 6

Related works on SOA impairment compensation

Compensation of SOA induced distortion, in particular through DSP implementation, is an active research topic. The most common approach followed is a post-compensation scheme, which proved to achieve good results in specific conditions [3–6, 18]. Many different implementations of such a method are possible depending on the model used to describe the SOA operation. Some of these possibilities, together with the specific conditions in which they have been applied, are here reported and compared to what has been developed in this thesis.

6.1 Digital back propagation based on Noisy Cassioli-Mecozzi model

In [3, 4, 18] the Noisy Cassioli-Mecozzi model [19] is used to build a post-compensation scheme. This model is partially based on the same rate equation used in this thesis to evaluate the spatially averaged integrated gain h but it includes also a model for ASE. These formulae are not used directly as input-output relations but instead are applied on different spatial sections of the SOA, providing a segmented model. In [3] two different possibilities are proposed and tested. The first one is based on a Runge-Kutta 4th order implementation of the model just described and it is referred to as RK4BP. The other solution, based on designing a first order digital filter starting from the full model, is characterised by reduced algorithmic complexity. This method is referred to as DFBP.

These implementations are tested on 16-QAM signals, with variable input power and OSNR after the transmitter, leading to the results in figure 6.1. The BER is improved of around two orders of magnitude for an input power of -8 dBm, similar to the one used in the simulations performed in this thesis. The first order method DFBP in particular provided promising results if related to its very low algorithmic complexity. Anyway it must be noted how these results are obtained with 16-QAM signals. For this modulation format also in the simulations performed in this work the outcome was much more promising than for 64-QAM, which was the main focus of this work.

Moreover looking at figure 6.2, where in the SOA a fixed current of 200 mA is injected and the OSNR after the transmitter is 45 dB, only for input powers of −10 dBm or lower the method proves to provide a BER lower than the Forward Error Compensation (FEC) limit.

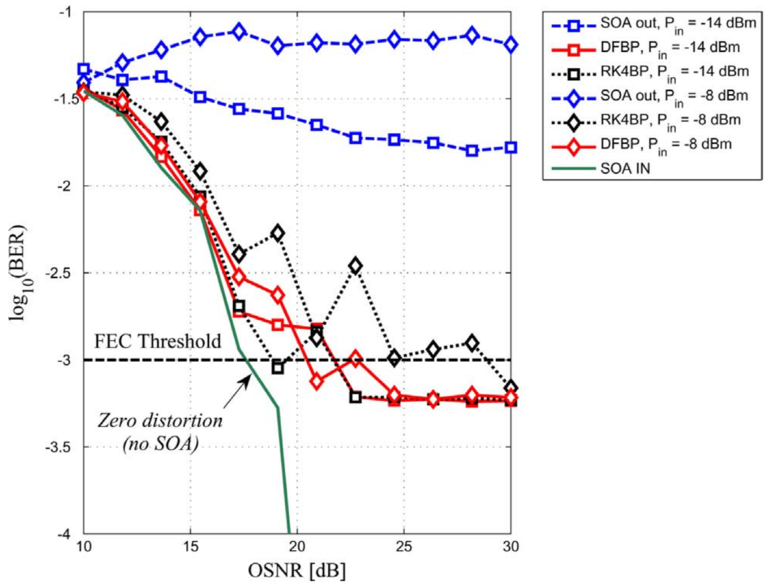

Figura 6.1. Obtained BER with variable OSNR and input power for a 16-QAM signal. Figure from [3].

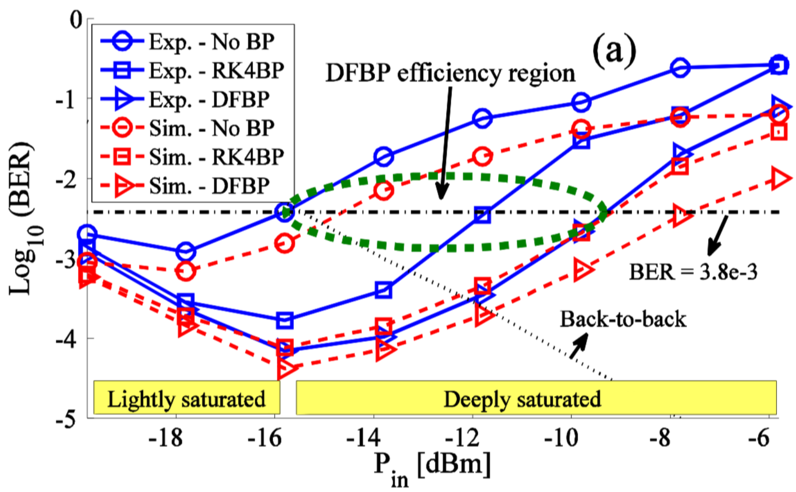

Figura 6.2. Obtained BER with variable input power for a 16-QAM signal. Figure from [4].

6.2 Experimental results for post-compensation method

An approach similar to the one of chapter 4 for developing the post-compensation has been followed in [5, 6]. In [5] in particular the method has been tested for OOK and 16-QAM signal with the inclusion of a 100 km long fiber. The block diagram of the experimental setup is shown in figure 6.3, where VOA stands for Variable Optical Attenuator and BPF for Band Pass Filter. The experiment demonstrated that digital post-compensation of both SOAs induced impairments and fiber distortion can work simultaneously. In [6] the same mathematical framework is implemented through a training based, adaptive device parameter estimation whose block diagram is reported in figure 6.4. The three unknown parameters g_0, τ_c, P_{sat} are fit through a known input E_{ts}. The bit sequence of this signal is completely random in order to adapt to the pattern effect in as many conditions as possible. This method has been tested with 16-QAM signals characterised by $P_{in,av} = -12.20$ dBm and a baud rate of 32 GBd/s. The SOA gain was varied between 15 dB and 20 dB while the sampling rate was 80 GSa/s. The OSNR has instead not been specified. In these condition a maximum improvement of the Q-factor of 2.52 dB has been obtained.

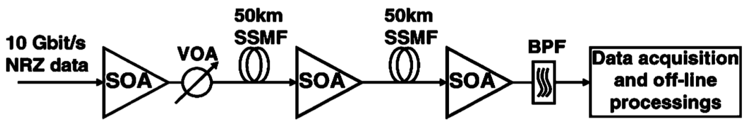

Figura 6.3. Experimental setup for SOAs distortion and fiber dispersion compensation. Figure from [5].

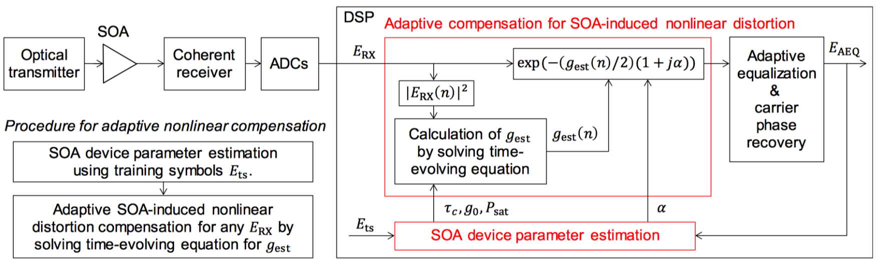

Figura 6.4. Block diagram for SOAs distortion compensation with adaptive parameters estimation. Figure from [6].

6.3 Contribution of this thesis to the topic

All the works discussed in this chapter have been focused on 16-QAM signals. Anyway, with the increasing need in improving the channel capacity, the use of higher order modulations such as 64-QAM is becoming of interest. This was then the main simulation objective of the thesis. Moreover most of the work related to DSP based SOA distortion compensation is actually based on post-processing. In section 4.3 of this work, on the other side, pre-compensation proved to be also a promising solution, able to overcome some of the limitations characterising data processing at the receiver stage.

Capitolo 7

Conclusions

In this thesis the distortion introduced by SOAs in coherent optical communication systems has been extensively treated. After having provided a general overview of the full system and a theoretical background regarding the device under study, a computationally efficient model has been built to numerically analyse the problem. This step was followed by a validation process, apt to corroborate the quality of the results obtained and to define the working region in which the model is applicable, regarding both device and system parameters. This step has been accomplished through simulations and comparisons performed with a well established commercial software: VPIphotonics Design Suite.

Given the positive results obtained during the validation phase, the model has been first exploited for a complete parametric study of the saturation characteristics achievable in SOAs, and then for developing a non linear compensation method. This last was first implemented through post-processing and proved to be an effective way of reducing the BER at the receiver stage also when tested in realistic situations, with a reduced number of samples available and in presence of noise.

The same mathematical framework has been also exploited to develop a pre-compensation method, which showed even better results and introduced a new level of flexibility with the possibility of correcting the distortion at the transmitter stage. This bonus being obtained at the cost of implementing DSP also in this stage and not only in the coherent receiver, with all the related consequences regarding increased system complexity and power consumption. These pre/post-compensation methods have shown, through simulations on 64-QAM signals, how their implementation in a communication network can dramatically decrease the BER, making feasible to transmit high order modulated signals to improve the channel capacity with respect to the actual standards.

Finally other two compensation methods, based on linear filtering and voltage driving of the SOA, have been discussed. The advantage of these is that they do not require the introduction of DSP routines. Unfortunately, in this cases, not promising results have been obtained. The attempted linear filtering proved to be not adequate for correcting intensity modulated signal, since it alters the power level ratio between different transmitted levels. Voltage driving, on the contrary, showed impressive potentialities in theory but practical limitations, given by the device fabrication process, make it infeasible.

Bibliografia

[1] Michael J Connelly. *Semiconductor optical amplifiers*. Springer Science & Business Media, 2007.

[2] Govind P Agrawal and N Anders Olsson. Self-phase modulation and spectral broadening of optical pulses in semiconductor laser amplifiers. *IEEE Journal of Quantum Electronics*, 25(11):2297–2306, 1989.

[3] Amirhossein Ghazisaeidi and Leslie Ann Rusch. On the efficiency of digital back-propagation for mitigating soa-induced nonlinear impairments. *Journal of Lightwave Technology*, 29(21):3331–3339, 2011.

[4] Siamak Amiralizadeh, An T Nguyen, Chul Soo Park, Amirhossein Ghazisaeidi, and Leslie Rusch. Experimental validation of digital filter back-propagation to suppress soa-induced nonlinearities in 16-qam. In *Optical Fiber Communication Conference*, pages OM2B–2. Optical Society of America, 2013.

[5] Xiaoxu Li and Guifang Li. Electrical postcompensation of soa impairments for fiber-optic transmission. *IEEE Photonics Technology Letters*, 21(9):581–583, 2009.

[6] Fukutaro Hamaoka, Seiji Okamoto, Masanori Nakamura, Asuka Matsushita, and Yoshiaki Kisaka. Adaptive compensation for soa-induced nonlinear distortion with training-based estimation of soa device parameters. In *2018 European Conference on Optical Communication (ECOC)*, pages 1–3. IEEE, 2018.

[7] Ke Wang, Jie Li, Anders Djupsjöbacka, Sergei Popov, Gunnar Jacobsen, Robert Elvis Makon, Rachid Driad, Herbert Walcher, Josef Rosenzweig, Andreas G Steffan, et al. 100 gb/s rz-ook transmission through 212 km deployed ssmf using monolithically integrated etdm receiver module. *Optics Communications*, 284(3):782–786, 2011.

[8] Matthias Seimetz. Multi-format transmitters for coherent optical m-psk and m-qam transmission. In *Transparent Optical Networks, 2005, Proceedings of 2005 7th International Conference*, volume 2, pages 225–229. IEEE, 2005.

[9] Matthias Seimetz and C-M Weinert. Options, feasibility, and availability of 2/spl times/4 90/spl deg/hybrids for coherent optical systems. *Journal of lightwave technology*, 24(3):1317–1322, 2006.

[10] Mads L Nielsen, Kiyotaka Tsuruoka, T Kato, T Morimoto, Shinya Sudo, Takeshi Okamoto, Kenji Mizutani, H Sakuma, Kenji Sato, and Koji Kudo. Soa-booster integrated mach–zehnder modulator: investigation of soa position. *Journal of Lightwave Technology*, 28(5):837–846, 2010.

[11] Larry A Coldren, Scott W Corzine, and Milan L Mashanovitch. *Diode lasers and photonic integrated circuits*, volume 218. John Wiley & Sons, 2012.

[12] Michael J Connelly. Wideband semiconductor optical amplifier steady-state numerical model. *IEEE Journal of Quantum Electronics*, 37(3):439–447, 2001.

[13] Prashant P Baveja, Drew N Maywar, Aaron M Kaplan, and Govind P Agrawal. Self-phase modulation in semiconductor optical amplifiers: impact of amplified spontaneous emission. *IEEE journal of quantum electronics*, 46(9):1396–1403, 2010.

[14] Niloy K Dutta and Qiang Wang. *Semiconductor optical amplifiers*. World scientific, 2013.

[15] Jia Dong. *Estimation of Bit Error Rate of any digital Communication System*. Télécom Bretagne, Université de Bretagne Occidentale, 2013.

[16] Yan Han and Guifang Li. Noise statistics of and ber estimation using demodulated signals for direct detection differential polarization-phase-shift keying. *Optics Express*, 13(7):2761–2766, 2005.

[17] M Nadeem Akram, Richard Schatz, and Olle Kjebon. Influence of electrical parasitics and drive impedance on the laser modulation response. *IEEE Photonics Technology Letters*, 16(1):21–23, 2004.

[18] Francesco Vacondio, Amirhossein Ghazisaeidi, Alberto Bononi, and Leslie Ann Rusch. Low-complexity compensation of soa nonlinearity for single-channel psk and ook. *Journal of Lightwave Technology*, 28(3):277–286, 2010.

[19] Cristian Antonelli and Antonio Mecozzi. Reduced model for the nonlinear response of reflective semiconductor optical amplifiers. *IEEE Photon. Technol. Lett*, 25(23): 2243–2246, 2013.